THERMAL PERFORMANCE OF FIRE PROTECTION MATERIALS

Zourkane Abdelkader

Final thesis submitted to the

School of Technology and Management

Polytechnic Institute of Bragança

For the fulfilment of the requirements for a Master's Degree in

Industrial Engineering

Mechanical Engineering Branch

July, 2017

THERMAL PERFORMANCE OF FIRE PROTECTION MATERIALS

Zourkane Abdelkader

Final thesis submitted to the

School of Technology and Management

Polytechnic Institute of Bragança

For the fulfilment of the requirements for a Master's Degree in

Industrial Engineering

Mechanical Engineering Branch

Supervisor at IPB:

Prof Dr. Luis Mesquita

Supervisor at UHBC:

Dr. Abdellah Benarous

July, 2017

ACKNOWLEDGEMENTS:

I would like to express my gratitude and appreciation to Professors Luis Mesquita and Abdellah Benarous for their excellent guidance, supervision, dedication and support throughout this year. The advices and comments of both professors that have been a considerable help and of great value for the successful and conclusion of this work.

Special thanks go to my family and friends for their continuous support and patience. I would like to thank the Erasmus + ICM, Internship and double diploma award between the Polytechnic Institute of Bragança (IPB) and the University Hassiba ben Bouali de Chlef (UHBC).

Thank you for your helpful technical advice, your support and encouragement during this period, for your cheerfulness, patience and love; thank you for always being at my side.

Fruitful result would not hasten without the moral support and encouragement of my family, my lovely and beautiful mother Lalia, my father Ahmed, my brothers Taher and Moussa and my sisters Aicha and Hadjer, that have enabled me to achieve this today.

Friendship is a wonderful blessing from God, I am blessed with my friends Thabet Ridha, Rami, Mohamed, Billel, Houssin, Soufyane, Hakima, Sabrina, Habib, Djilali, Hakim, Amhamed, Khaled, Belkacem, Jhony Lima, Hasmik, Seddik, Yassin, Younes, Youssef, Yasser, Abdelrahman, benouda, Amin, Khalil, Remdan, Lid, Nasser, Meloud, Howari, Aboubakr, Saif dean, Ferdous and Khaled for their moral support and encouragement, I am so glad to share this experience with you.

Finally, all the thanks to Allah for giving me the energy and the motivation to complete this thesis with your beautiful smiles.

Resumo

O método mais comum de se obter a resistência ao fogo requerida é através do uso de sistemas passivos de proteção contra fogo, nos quais o material mais utilizado são as placas de silicato de cálcio.

A utilização do Eurocódigo 3 parte 1.2 para a evolução da temperatura do aço dos elementos protegidos contra o fogo requer o conhecimento das propriedades térmicas dos materiais aplicados em função da temperatura. Normalmente, estas propriedades não são conhecidas para todos os materiais e nem para toda a gama de temperaturas necessárias na verificação de segurança ao fogo.

O objetivo deste trabalho é desenvolver um conjunto de testes experimentais realizados com o objetivo de caraterizar a eficiência térmica durante a sua exposição a temperaturas elevadas. Os testes são conduzidos num calorímetro de cone usando diferentes espessuras de placas de aço e espessuras de placas de isolamento e fluxos de calor por radiação. Os resultados dos testes experimentais são comparados com os obtidos a partir de resultados numéricos usando o método de diferenças finitas, implementado em Matlab. Uma atenção particular é dedicada à modelação numérica das reações químicas e da evaporação da água devidas ao aumento da temperatura do material de isolamento, placas de silicato de cálcio.

Os resultados mostram a comparação entre as temperaturas medidas na chapa de aço carbono expostas a temperatutras elevadas e as temperaturas obtidas pelo método simplificado do Eurocódigo e pelo modelo numérico, seguem a mesma tendência. A diminuição da temperatura do aço ocorre com o aumento da espessura da placa de aço carbono, do fluxo de calor e com o aumento da espessura das placas de isolamento.

Palavras-chave:

Resistência ao fogo; Proteção ao fogo; Propriedades térmicas; Testes experimentais.

Abstract

The most common method of achieving the required fire resistance is by the use of passive fire protection systems, in which the most common material calcium silicate board is used.

The use of the Eurocode 3 part 1.2 for the steel temperature evolution of fire protected elements require the knowledge of the thermal properties of the applied materials in function of the temperature. Usually these properties are not known for all the materials and not for all the temperature range needed for fire design.

The aim of this work is to develop an experimental set of tests made with a fire insulation material in order to characterize the thermal efficiency during the temperature exposure. Tests are made in a cone calorimeter using different steel plate thickness, insulation plate thickness and radiative heat fluxes. The experimental tests results are compared with the one obtained from numerical results using the finite difference method by implementing in Matlab. Special care is made to include the chemical reactions and evaporation of water from the heating of the insulation material, calcium silicate boards.

Results showed the comparison between the measured temperatures in carbon steel plate exposed to fire and the corresponding calculated temperatures presented a very good agreement and the decrease in the temperature vary with the increase of the thickness of carbon steel plate and heat flux and the fire insulation boards.

Keywords:

Fire resistance, Fire protection, Thermal properties, Experimental Tests.

INDEX

LIST OF FIGURES

LIST OF TABLES

SYMBOLOGY

LATIN UPPERCASE LETTERS

A_m /V	is the section factor
A_p	is the appropriate area of fire protection material per unit length of the member [m²]
Ksh	is the correction factor for shadow effect
N	is the number of grid points
T	is the temperature
T_g	is the gas temperature in the vicinity of the fire exposed member
T_s	is the surface temperature of the member
UNP	is the unprotected steel plate
X_L	is the left boundary condition
X_R	is the right boundary condition

LATIN LOWERCASE LETTERS

c_a	is the specific heat of steel
c_p	is the specific heat of insulation

d_p	is the thickness of fire protection material
d_s	is the thickness of steel
dt	is the time interval
f	is the spatial differential operator
$\dot{h}_{\text{net}}$	is the net heat flux
$\dot{h}_{\text{net,r}}$	is the net radiative heat flux
$\dot{h}_{\text{net,c}}$	is the net convective heat flux per unit surface area
i	is the spatial grid points
q'''_{gen}	is the generation function
t	is the time
u	is the vector of dependent variables
$\mathbf{u}_t$	is the first order partial deriavative of u with respect to t
$\mathbf{u}_x$	is the first order partial deriavative of u with respect to x
x	is the boundary value independent variables

GREEK UPPERCASE LETTERS

Δx	is the distance between grid points
Δt	is the time interval
$\Delta T_{s,t}$	is the increase of the ambient steel temperature during the time interval Δt
$\emptyset$	is the configuration factor

GREEK LOWERCASE LETTERS

α is the coefficient of heat transfer by convection

ρ_s is the unit mass of steel

ρ_p is the unit mass of the fire protection material

ε_s is the surface emissivity member

ε_f is the emissivity of the fire

σ is the Stephan Boltzmann ($= 5{,}67.10^{-8}[W/\mathrm{m}^2\mathrm{K}^4]$)

λ_p is the fire protection system

v is the velocity

Chapter 1: MOTIVATION AND OUTLINE

1.1 Motivation

The most fundamental block building constructures nowadays are safety particularly the fire safety requirements of design. Saving human life is the aim of fire safety. Nevertheless, minimizing the financial loss incurred as a result of damage to properties and contents should be considered.

There are many different techniques to reduce the risk of fire; it can be by including fire management department in order to minimize occurrence of ignition and control of combustible materials. However, the design of buildings has great effect of controlling fires when it takes place. Forcing the governments in terms of regulations and insurance conditions can be helpful to reduce the risk of fire.

The basic and most widely used technique is adding and using calcium silicate board a fire resistance material in the building structures. Those materials help the structures to hold under extreme high temperatures until firemen arrive. Great example of the effect of considering fire resisting materials is the last incident that took place at apartment tower in London. It started with a small fire, but the building could not hold because there were no fire resistance materials in the design of the building; in result, twelve civilians were dead and losing everything inside the building.

1.2 Objective

The main target of our work is to make experimental tests for protected and unprotected steel plate with different insulation, different thickness steel plate and different heat flux in cone calorimeter. For the protected carbon steel plate, two different insulations are used named Promatect-H and Promatect-200 (Calcium Silicate Board) with different thickness.

1.3 Outline

Chapter 2: A general review of the recent works is presented in the state of the art

Chapter 3: Presents the simple method of Eurocode 3 part 1.2

Chapter 4: The experimental tests for unprotected and protected carbon steel plate with different insulation PROMATECT-H and PROMATECT-200 in high temperature

Chapter 5: Presents the numerical solution using method of lines (MOL) in finite difference method, compared with experimental result

Chapter 6: Represents the main conclusions of this work and proposed some suggestions for future work

Chapter 2: STATE OF THE ART

The main published works are about using different insulation materials for supporting building structures. Where, the properties of insulation material were studied in different experimental conditions. Those studies are presented in Table 1.

Table 1 - Recent publications on insulation materials

Author	Year	Study	Software/Method	Insulation Material	Building Structures
Thomas	2002	Thermal properties of gypsum plasterboard at high temperatures, thermal conductivity	TASEF ABAQUS	Gypsum plasterboard	Modelling of thermal behaviour for fire resistance
Bartholmai *et al*	2003	Influence of heat flux thermal insulation properties, cone-calorimeter tests	IOPT2D FORTRAN	Polymeric intumescent coatings	Steel Plates
Adl-Zarrabi *et al*	2006	Determining the thermal properties of concrete and wood	TPS method	Concrete and wood	-
Chi *et al*	2007	Microstructure and thermal conductivity of hydrated calcium silicate board	Hot Disk computer software	Calcium silicate board	Sicrostructure of steel
Kodur and Shakya	2013	Effect of temperature on thermal properties of spray applied in fire resistive materials	Hot Disk computer software; ANSYS program	Spray applied fire resistive materials; Gypsum	Steel structures
Elliott *et al*	2014	Novel testing of intumescent coatings under non-standard heating regimes	Furnace; thermal imaging camera	Reactive coatings	Steel structures
Qiang Li *et al*	2016	Predicting steel temperature using constant thermal conductivity	Big furnace	Intumescent coating	Steel plate
Mróz *et al*	2016	Material solutions for passive fire protection of buildings	-	Concrete; Gypsum	Structural steel element, electrical installation
Ferreira *et al*	2017	Behaviour of non-loadbearing tabique wall subjected to fire – experimental and numerical analysis	Fire-resistance furnace; numerical models	Tabique wall	Pine wood

A thermal study of properties for gypsum plasterboard at high temperatures was published by Geoff Thomas in 2002 [1]. In that work, the determination of thermos-physical properties of gypsum was done in order to estimate the thermal behaviour, a review of dehydration reactions of gypsum undergoes in terms of heating situations were considered. There was a great agreement of the enthalpy and thermal conductivity curve for input into a finite element heat transfer model, an engineering plasterboard product was tested in that work, the values of conductivity of gypsum plasterboard at very high temperatures and specific heat had been modified to some extent in the calibration of the heat transfer model. However, they found that the heat transfer model has some limitations, such as the inability to model mass transfer, the movement of moisture and pyrolysis products through the wall materials and across the void.

Another study was published by Bartholmai *et al* in 2003, it was about the effect of external heat flux and coating thickness on the thermal insulation. In that work, they found that using a polymeric intumescent coating is allowing a better resistance when exposed to high temperatures. Nevertheless, it protects the structures from damage, [2].

Another published work by Adl-Zarrabi *et al* 2006, about the use of TPS method to determine the thermal properties of materials at room temperature as well as a higher temperature up to 700 [ºC], [3]. In that study, wood and concrete were used in order to determine the thermal properties named conductivity and diffusivity. A comparison between the predicted results and some values in literatures were studied.

Kodur and Shakya reported in 2013, they studied the thermal properties of fire insulation such as thermal conductivity, specific heat and thermal strain were done to improve fire resistance of steel structural members, [4]. The effect of temperature on thermal properties of different types of spray applied fire resistive materials were studied in that work. They found that the temperature has significant effect on thermal conductivity, specific heat, thermal strain and mass loss of spray applied in fire resistive materials.

In 2016 Mróz *et al* published a report with the main focus of the thermal properties of passive fire protection materials under test with high temperature or in fire conditions, the main objective of that work was to see thermal insulation barrier, endothermic building materials including concrete and gypsum and also a novel solution based on alkali activated binders, [5]. A different type of passive fire protection materials were mentioned such as

mineral wool, perlite, shale, clay, slate and vermiculite, and the cellulose insulation which is made in a loose form from a recycled paper, newspaper, cardboard or other similar materials, concrete and gypsum plus the intumescent and ablative materials.

Another study in 2016 was carried out by Qiang *et al* by using constant thermal conductivity, they found that it was protecting the steel temperature in fire together with intumescent coating. In that work, they used analysing of a series of fire tests on intumescent coating protected steel sections with a range of section factors and intumescent coating thicknesses, [6].

Recently, in another work reported by Ferreira *et al* in 2017 [7], the study was about the fire resistence of non-loadbearing tabique wall containing an experimental program including tabique panels which represents a portion of a real-scale wall and all the dimensions are real one, manufactured in laboratory made in pine wood with an earth-based render finishing. In order to assess the thickness effect of the earth-based render on the fire resistance of the wall, three specimens with different render thicknesses of 15 [mm], 10 [mm] and 5 [mm] were tested in a fire-resistance furnace according to the ISO 834 standard fire curve. Two performance criteria were verified which were the integrity and the insulation. In addition, a numerical model was also developed in order to assess the tabique wall behaviour under fire conditions, which was validated using the obtained experimental results. The insulation criterion between the average temperature increase and the average initial temperature was not higher than 140 [°C] and the maximum temperature at any point of the unexposed surface did not exceed the final temperature of 180 [°C]. The tabique walls behaviour was similar in all experimental tests, the temperature evolution was more pronounced in tabique panel with thinner render layer. The numerical temperatures show good agreement with the experimental results (temperature and position of the char layer). The numerical models were validated experimentally allowing calibrating and adjusting the material properties used in the tabique wall panels after measuring elevated temperature in TPS for the specimen they compared the result with the results obtained by the MDSC technique.

Chapter 3: SIMPLE METHOD OF EUROCODE

3.1 Introduction

This chapter study numerical result for unprotected and protected carbon steel plate by using eurocode 1993 part 1.2 for the insulation using thermal properties for gypsum board.

Firstly, it is necessary to write the equation for the steel plate temperature development.

3.2 Steel temperature development unprotected internal steelwork

For an equivalent uniform temperature distribution in the cross-section, the increase of temperature ($\Delta T_{s,t}$ [k]) in an unprotected steel member during a time interval (Δt)[second] should be determined from Eq (1), [8].

$$\Delta T_{s,t} = Ksh \frac{A_m/V}{C_a \rho_s} h_{net} \Delta t \quad (1)$$

The increase of the temperature in an unprotected steel member during a time interval ($\Delta T_{s,t}$, expressed on [K]) depends on value of the net heat flux per unit area (h_{net} , expressed on [W/m^2]) and the specific heat of steel (C_a, expressed on [J/kgK]), the correction factor for the shadow effect ($Ksh = 1$), the section factor for the unprotected steel members (A_m/V expressed on $[1/m]$), the unit mass of steel (ρ_s =, expressed on [kg/m^3]) and the time interval (Δt, expressed in [seconds]).

On the fire exposed surfaces, (Using Eurocode 1 Part 1.2) the net heat flux (h_{net}) Eq (2), should be determined by considering heat transfer by convection and radiation as, [9].

$$h_{net} = h_{net,c} + h_{net,r} \quad (2)$$

$$h_{net,c} = \alpha_c(T_g - T_s) \quad (3)$$

$$h_{net,r} = \emptyset\varepsilon_s\varepsilon_f * 5{,}67.10^{-8} * \left[(T_g + 273)^4 (T_s + 273)^4\right] \quad (4)$$

Where the net convective heat flux ($h_{net,c}$ [w/m²]) Eq (3) and the coefficient of heat transfer by convection ($\alpha_c = 4\ [W/m^2K]$), the gas temperature in the vicinity of the fire exposed member (T_g) [°C] and the surface temperature of the member (T_s [°c]).

The net radiative heat flux ($h_{net,r}$ [w/m²]), Eq (4) determined by the configuration factor ($\emptyset$), the surface emissivity member (ε_s), the emissivity of the fire (ε_f), the Stephan Boltzmann ($\sigma = 5{,}67.10^{-8}[W/m^2K^4]$), the gas temperature to the fourth (T_g [K]), the steel temperature to the fourth (T_s[K]).

Specific heat is the measure of the materials ability to absorb heat. For steel, specific heat is a function of temperature and is independent of the composition of steel. The variation of specific heat with temperature is represented in Figure 1. The specific heat of steel C_a defined in accordance to CEN - EN 1993-1-2, as the following in Eq(5), (6),(7) and Eq(8), [8].

If $20°c <= T_s < 600°c$

$$c_a = 425 + 7{,}73.10^{-1} * T_s - 1{,}69.10^{-3} + 2{,}22.10^{-6} * {T_s}^{-3} \quad (5)$$

If $600°C <= T_s < 735°c$

$$c_a = 666 + 13002/(738 - T_s) \quad (6)$$

If $735°c <= T_s < 900°c$

$$c_a = 545 + 17820/(T_s - 731) \quad (7)$$

If $900°c <= T_s < 1200°c$

$$c_a = 650 \quad (8)$$

Where, T_s is the steel temperature[°c]

Figure 1 shows variation of the specific heat with temperature.

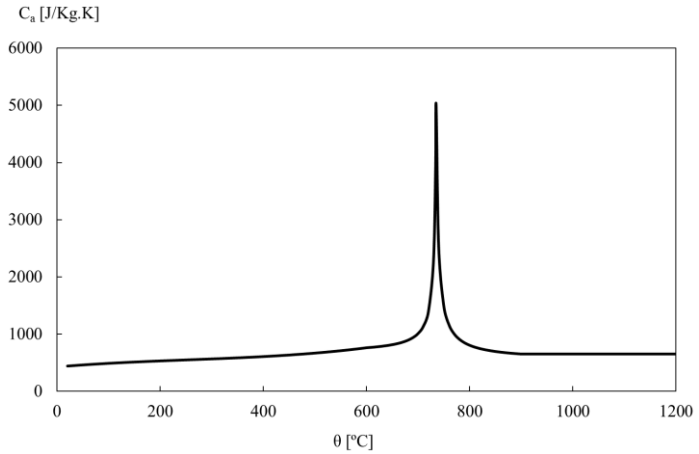

Figure 1: Specific heat of carbon steel as a function of the temperature, [8].

For a uniform temperature distribution in a cross-section, the temperature increase ($dT_{s,t}$) ,Eq(9) of an insulated steel member during a time interval (dt) should be obtained from ,[8].

$$dT_{s,t} = \frac{\lambda_p A_p/V(T_{g,t}-T_{s,t})}{d_p c_a \rho_s (1+\emptyset/3)} dt - \left(e^{\frac{\emptyset}{10}} - 1\right) dT_{g,t}, \quad (9)$$

(but $dT_{s,t}$>0 if $dT_{g,t}$>0)

With $$\emptyset = \frac{c_p \rho_p}{c_a \rho_s} d_p A_p/V$$

Where the section factor for steel members insulated by fire protection material (A_p/V), the appropriate area of fire protection material per unit length of the member (A_p)[m²/m], the volume of the member per unit length (V) [m^3/m], the temperature dependent specific heat of steel, from section 3 (c_s expressed on [J/kgK]; the temperature independent specific heat of the fire protection material ($c_p = 1700$ [J/kgK]); the thickness of the fire protection material(d_p=5, 7.5 and 10[m]); the time interval (dt=5[seconds]); the steel temperature at time *t* ($T_{s,t}$ [°C]); the ambient gas temperature at time *t* ($T_{g,t}$ [°C]); the increase of the ambient gas temperature during the time interval ($dT_{g,t}$ [K]); the thermal

conductivity of the fire protection system (λ_p=02 [W/mK]); the unit mass of steel, from section 3 (ρ_s $[\frac{kg}{m^2}]$) and the unit mass of the fire protection material ($\rho_p = 800[\frac{kg}{m^2}]$).

3.3 Numerical result

After putting those equations from protected and unprotected steel members in Matlab (see ANNEX A1, A2) it gives us the result in graph below.

Figure 2 represents the temperature variation with time for the ISO-834 and unprotected steel plate, when the thickness of steel plate increases, in result the temperature decreases.

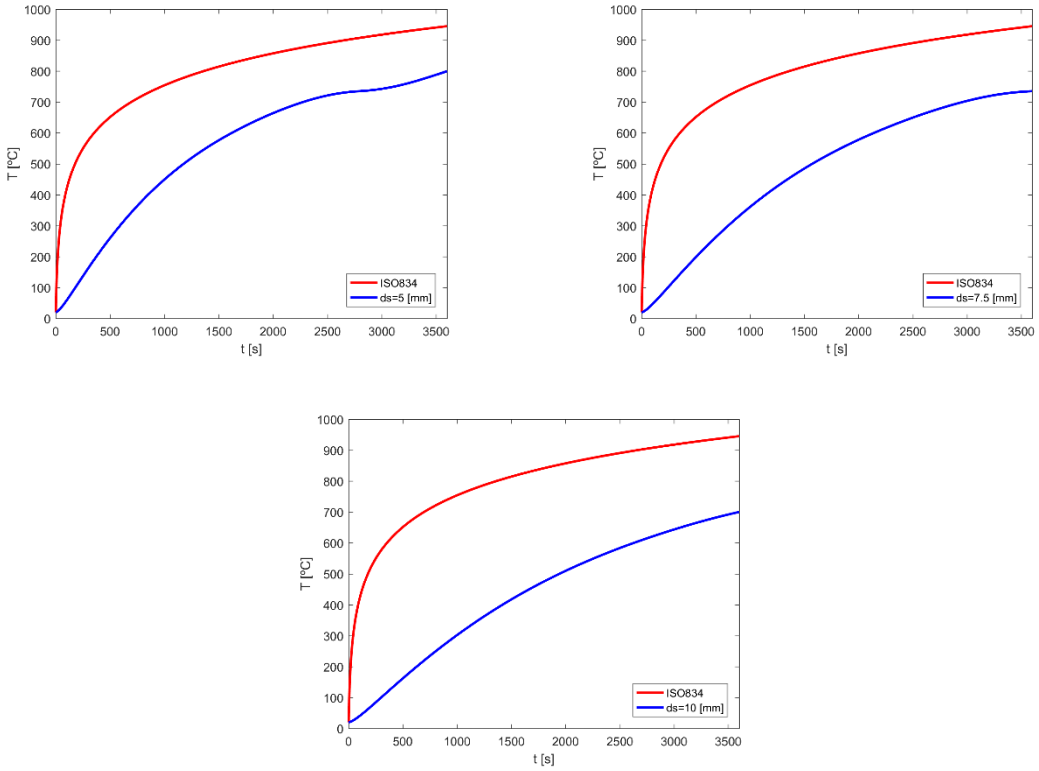

Figure 2 : The temperature variation with time for ISO834 and unprotected steel plate.

Figure 3, Figure 4 and Figure 5 shows the temperature variation with time for protected steel plate in the same thickness with different thickness of insolution. When the thickness of insulation increases, the temperature decreases.

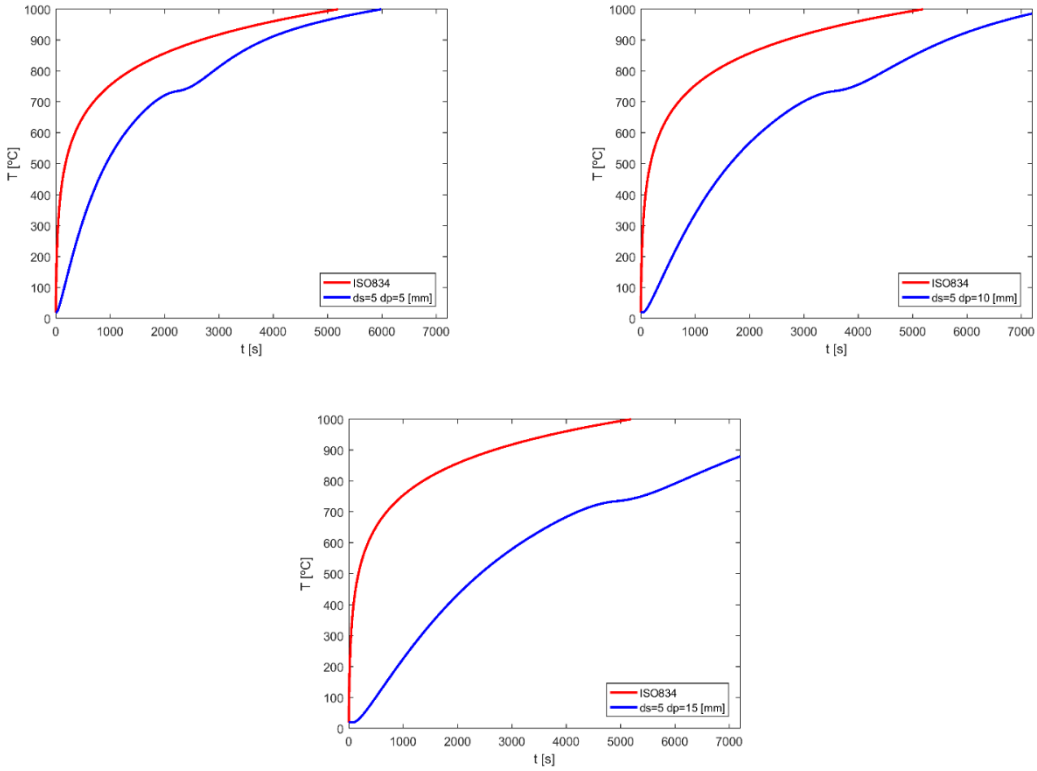

Figure 3 : The temperature variation with time for ISO834 and protected steel plate, ds = 5.

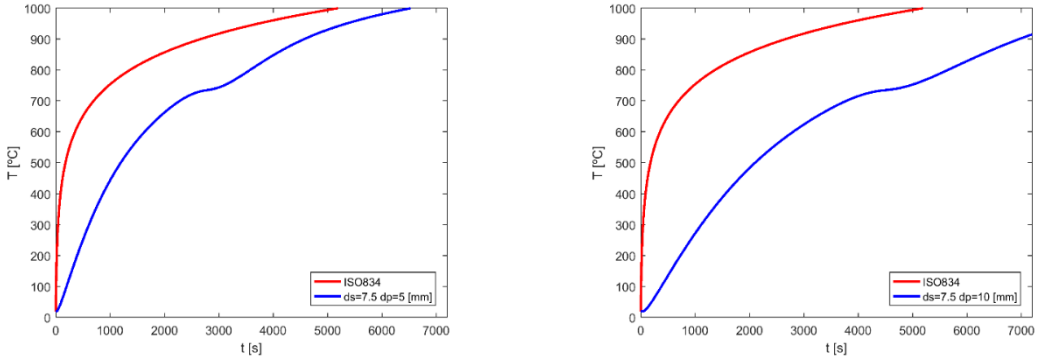

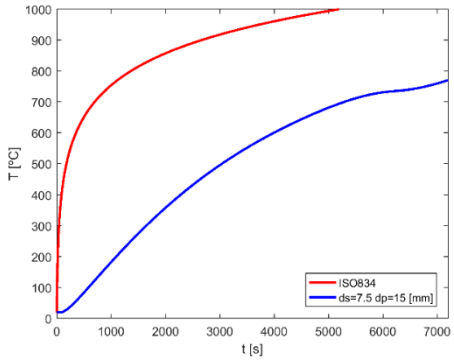

Figure 4 : The temperature variation with time for ISO834 and protected steel plate, ds = 7.5.

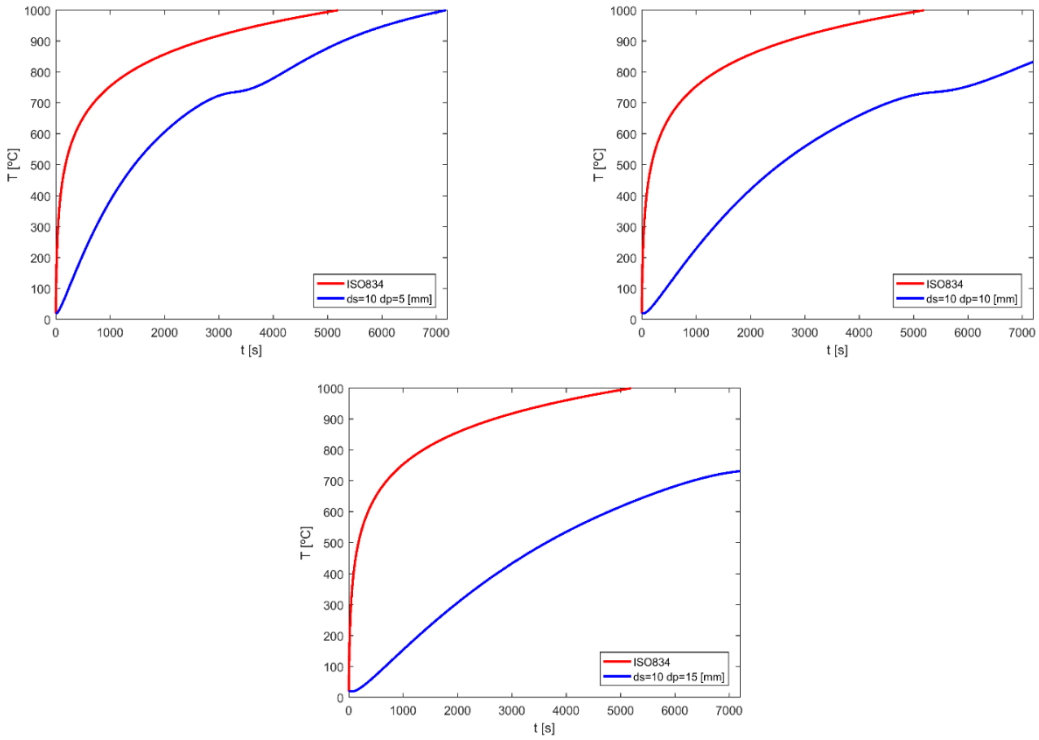

Figure 5 : The temperature variation with time for ISO834 and protected steel plate, ds = 10.

Table 2 shows the temperature variation with thickness of steel plate and thickness of insulation for protected and unprotected steel plate. For unprotected steel plate, it is seen that the temperature decreases when the thickness of steel plate increases and for 500[°c] the time increases when the thickness plate increases. On other hand, for protected steel plate it is seen that the temperature decreases when the thickness of insulation increases at the same thickness of steel plate. The time increases when the thickness of insulation increases in 5, 7.5 and 10[mm] thickness of steel plate.

Table 2 - Results of protected and unprotected steel in Matlab.

Case	ds [mm]	dp [mm]	time [s] 500 [°c]	time [s] 600 [°c]	Temp [°c] 1800 [s]	Temp [°c] 3600 [s]
1	5	/	518.3	680.1	828.8	942
2	7.5	/	651	835.5	805.4	940.2
3	10	/	769.3	975.8	768.4	938.2
4	5	5	925.5	1278.0	698	879.9
5	5	10	1645	2200	531	736.7
6	5	15	2415.8	3170.2	395.9	646.5
7	7.5	5	1193.4	1631.6	630.7	803.5
8	7.5	10	2100	2800.1	447.4	685.3
9	7.5	15	3034.3	3989.5	325.7	562.4
10	10	5	1444.3	1962.8	57.9	747
11	10	10	2532.2	3370.2	386.5	623.1
12	10	15	3627.7	4771.7	277.8	497.2

Where ds is the thickness of the steel plate and dp is the thickness of the insulation

Chapter 4: CONE CALORIMETER EXPERIMENTAL TESTS

4.1 Introduction

The cone calorimeter is a fire testing device based on the principle of oxygen consumption during combustion, used to study the fire behaviour of small samples of various materials in condensed phase, and this device is used by the most leading fire research groups as a data source for properties of materials and as a source for inputting data to models when predicting fire behaviour. It gathers data regarding the ignition time, mass loss, combustion products, heat release rate and other parameters associated with its burning properties, (see Figure 6).

Figure 6: Picture of the Cone Calorimeter.

The calcium silicate board is a Light silicate fire resistant construction board with PROMAXON® binder, has resistant to moisture, [10]. The calcium silicates are high performance where low density calcium silicate boards are very efficient insulating products, the special they have a low thermal conductivity which leads to low heat losses and these materials are stable up to 1050 °C and classified as A1, non-combustible according to EN 13501-1 and building material class DIN 4102, [calcium silicate insulation]. And It is produced with quality assurance according to the standard ISO 9001. About the field of using

this application is performance of construction materials for construction and technical fire protection in according to EN standard in all the fields of building construction and industrial construction, [11].

In this chapter, we talk about the result of the experimental test and the steps for how to make the test, we use the cone calorimeter to measure the temperature according to specimen. For the specimen, we have different carbon steel plate where they have 3.6, 7.75 and 14 [mm] thickness, the first step is, we test unprotected carbon steel plate and the second step is we test the protected carbon steel plate with two different insulation named promatect-200 and promatect-H. They have different thickness of 15 and 20 [mm].

4.2 Preparation of the specimens

In this step, the specimens are prepared firstly, in total, the tests will be done on 3 carbon steel plates, with different thickness, with the dimensions of (100 × 100) [mm²]. To do this laboratory test four steps should be done, the first step should be the preparation of the carbon steel plates, then cleaning with using the grinder machine (Figure 7), the second step should be the welding of the two thermocouples in the top of the steel plate and another two in the bottom. Thirdly, put the plate in the ceramic blanket (see Figure 8) and the last step is the calibration of calorimeter.

a) Carbon steel plates b) Grinder machine

Figure 7: The materials used.

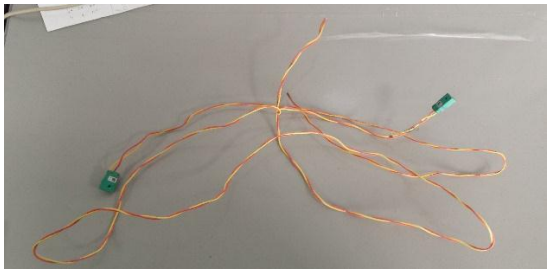

a) The thermocouples.

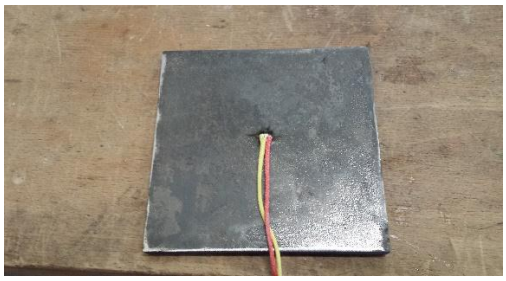

b) The thermocouples type K are welded in surface plate.

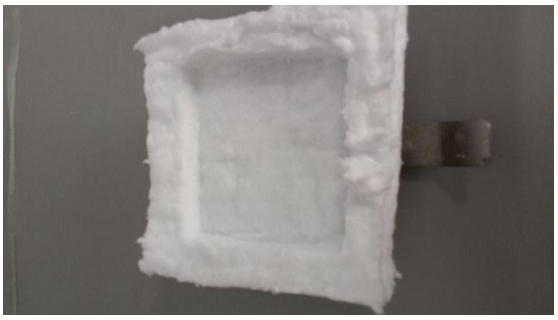

c) The ceramic blanket.

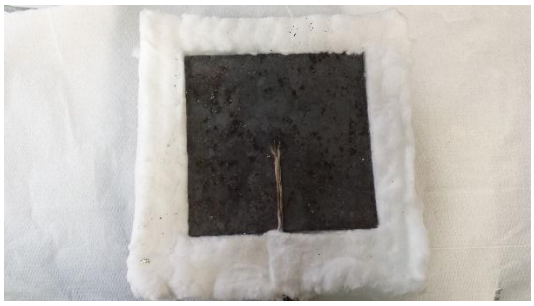

d) The prepared specimen.

Figure 8: The specimen of the unprotected carbon steel plate prepared.

4.3 Calibration of the cone calorimeter:

Before testing the specimens to give the required heat flux calibration is done according to the ISO 13927, [12]. This calibration is a process which consist to stabilize the heat flux using the temperature Figure 9. A heat flux meter is placed under the cone heater at the point corresponding to the centre of the specimen surface and the temperature controller adjusted until the required test heat flux is achieved, the three heat flux values needed are 35, 50 and 75 [kW/m^2] and in order, the three temperature values are 657, 749 and 867 [°C].

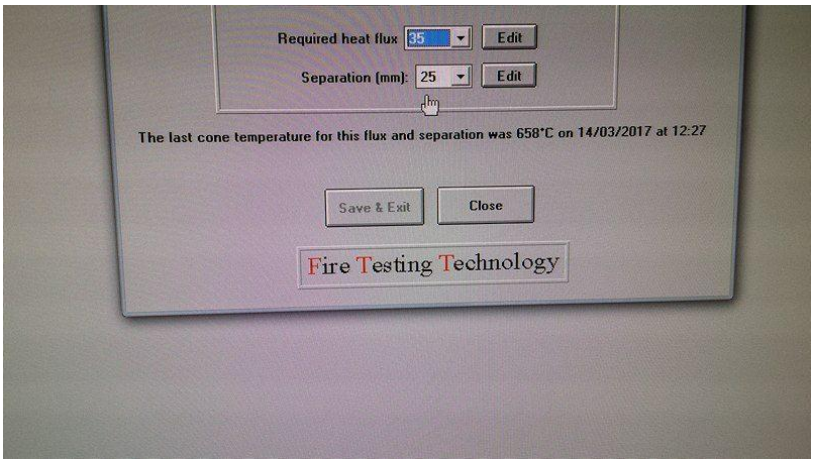

Figure 9 -: Programme MLCCalc to calibrate the cone calorimeter.

The Figure 10 shows schematic drawing of apparatus, where (1) Inner shell, (2) Refractory-fibre packing, (3) Thermocouple, (4) Outer shell, (5) Heating element and (6) Steel plate.

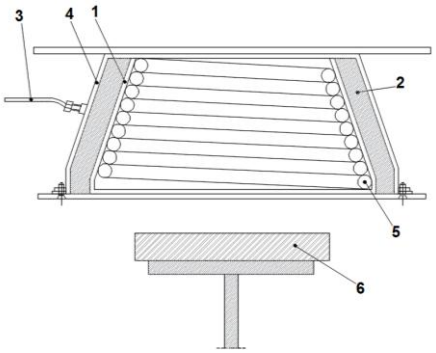

Figure 10: Schematic drawing of apparatus, [12].

4.4 Experimental tests for unprotected steel:

After preparing the specimens and calibrating the cone calorimeter, we start testing the specimens Figure 11, firstly set the distance between the bottom of the cone calorimeter and top of the specimen equal 15 [mm], secondly, turn on the cone calorimeter and the computer, after that start increasing the temperature of the cone calorimeter to reach the required heat flux. The spacimen is covered by heat isolant. We put it under the cone calorimeter, run the software with this and remove the isolant at the same time.

Figure 11: Cone calorimeter and experimental setup.

This result appears in excel after that we translate as a curve that is showing in Figure 12, Figure 13 and Figure 14 what express the variation of temperature in function with time

and heat flux. With the passage of time when the heat flux increases the temperature also increase.

For example, having a 3.6 [mm] thickness plate, in Table 8 we see that the maximum temperature for minimum heat flux (q=35 [kw/m²]) is 600 [°C]; furthermore, the temperature increase upto 800 [°C] when the maximum heat flux is (q=75[kw/m²].

The same result comes from different thickness plate what is shown below on Table 9 and Table 10.

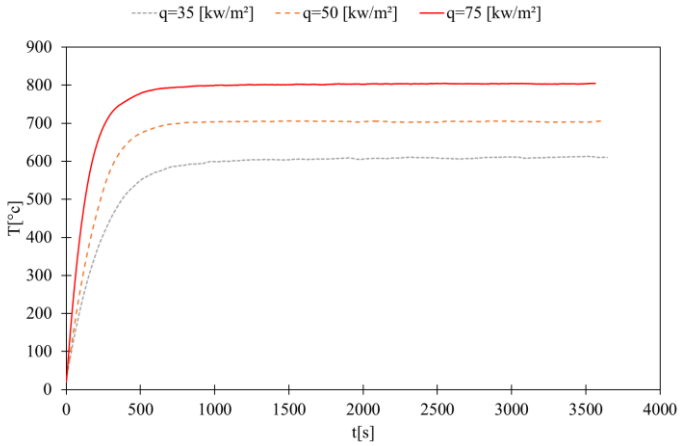

Figure 12: The temperature variation with time for the 3.6 [mm] thickness plate.

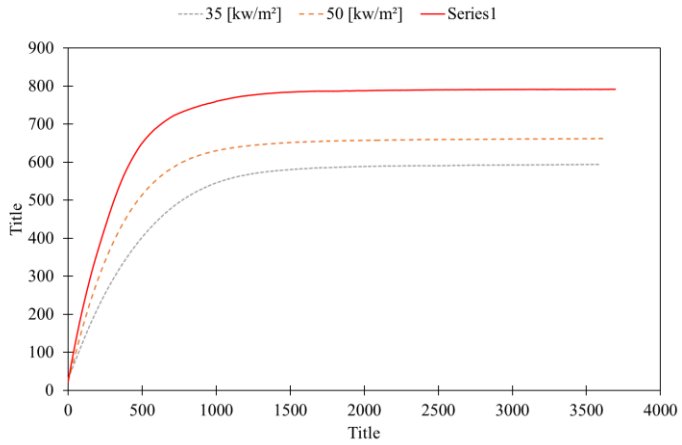

Figure 13: The temperature variation with time for the 7.75 [mm] thickness plate.

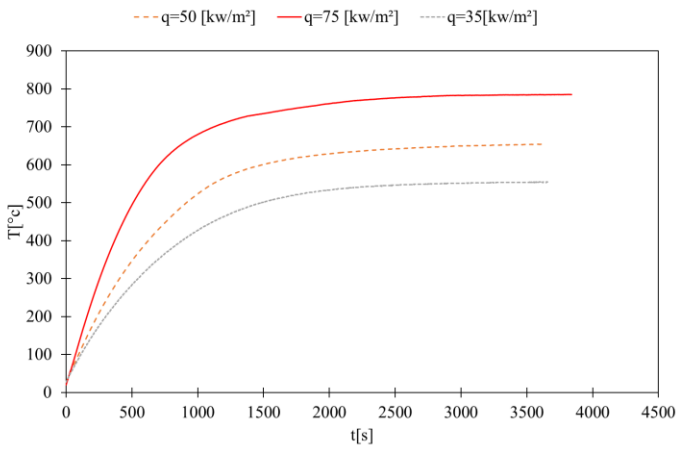

Figure 14: The temperature variation with time for the 14 [mm] thickness plate.

From the graphs of above figures, the following table is obtained that shows the behavior of the steel plate under high temperature, as it can be seen in the Table 3, at same time the temperature decreases when we increase the thickness of the carbon steel plate. And also, when we increase the thickness of the steel plate, the time increases in a selected temperature.

And in another side, in heat flux q=35 [kw/m²], for 3.6 [mm] thickness of steel plate, it has 593 [°c] decreasing to 292.81 [°c] when the thickness plate is increasing to 14 [mm] at the same time 900[s]; more, it takes 375.5[s] for 3.6[mm] thickness plate where for 14 [mm] it increases to 2267.5[s]. The same output will come for heat flux q=50 and q=75 [kw/m²] as well as.

Table 3 - Results of experimental test of unprotected steel plate.

q [kw/m²]	Ds [mm]	Taverage [°c]				time[s]			
		900 [s]	1800 [s]	2700 [s]	3600 [s]	300 [°c]	400 [°c]	500 [°c]	600 [°c]
35	3.6	593	607.1	607.24	610.55	152.5	241.5	375.5	1044.5
	7.75	528.99	585.68	591.16	594	315.5	494	769.5	/
	14	292.81	439.85	536.36	564.43	935	1527	2267.5	/
50	3.6	702.52	705.26	704.60	705.41	111.5	165	231	325.5
	7.75	619.99	656	660.38	662.58	209.5	318	470.5	770
	14	496.03	620.61	645.61	654.13	405	623	913	1488
75	3.6	798.99	802.42	804.05	805.05	63	91	126	175
	7.75	685	726.48	730.6	731.83	185.5	281	395	558
	14	659.81	752	779.80	785.33	254	367.5	508.5	705

4.5 Experimental tests for protected steel:

In this step, it's the same procedure for unprotected carbon steel plate; the difference is that we need to put the calcium silicate board in the upper side of the carbon steel plate in order to assure a protection, it has the same dimension with the carbon steel plate and two different calcium silicate board named PROMATECT-200 and PROMATECT-H, they have different thickness of 15 and 20 [mm], see

Figure 15.

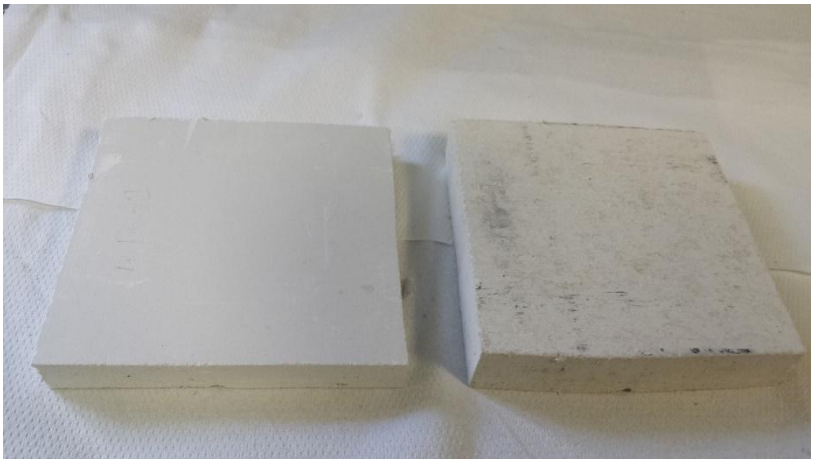

a) Two calcium silicate plates of different thickness: 15 and 20 [mm].

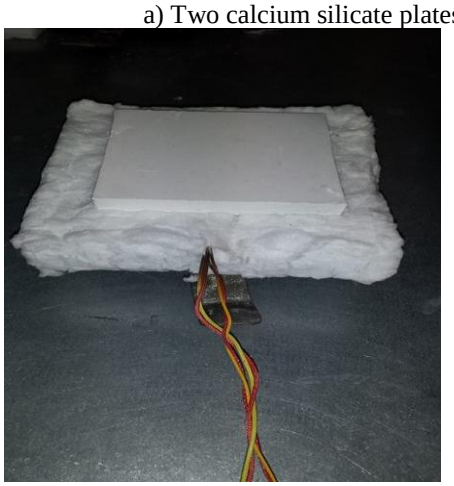

b) Protected carbon steel plate with calcium silicate 15 [mm].

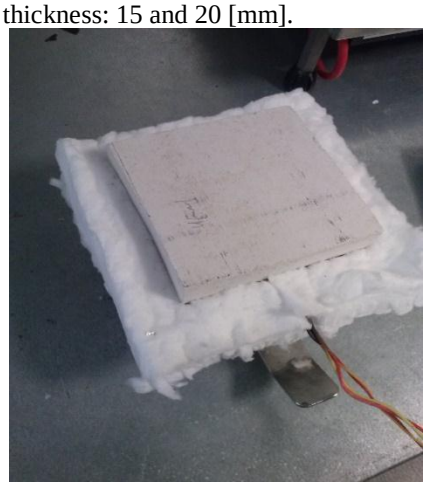

c) Protected carbon steel plate with calcium silicate plate 20[mm]

Figure 15: The specimen of the protected carbon steel plate prepared.

After preparing the specimen, we put it in the bottom of the cone calorimeter, where the distance is between the top of specimen and the bottom of the cone calorimeter is 25 [mm], see Figure 16.

Figure 16: Cone calorimeter and experimental setup.

4.6 Experimental tests for protected steel

About protected carbon steel plate with calcium silicate board which has 15 [mm] of thickness, by obtaining the following results transformed to graph in Figure 17, Figure 18 and Figure 19, it can be seen that the temperature of the steel plate increases slowly between 100 and 200 [°c] because the water starts to vaporize at 100 [° C]. After 200 [°c] we can see that there is a sharp increase in steel substrate temperature due to the total evaporation of water, [13].

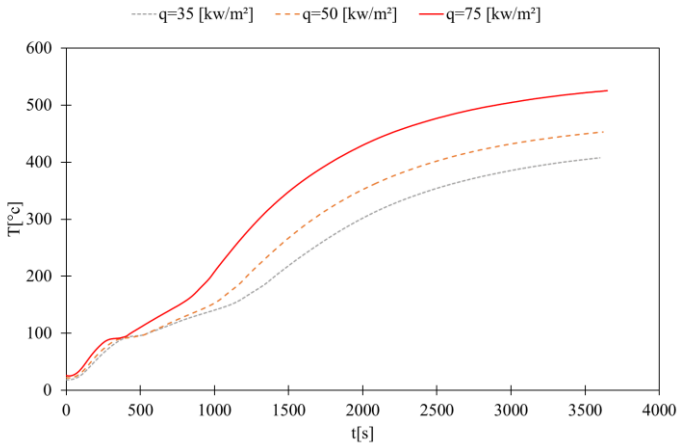

Figure 17: The temperature variation with time for the 3.6 [mm] thickness plate and dp 15 [mm].

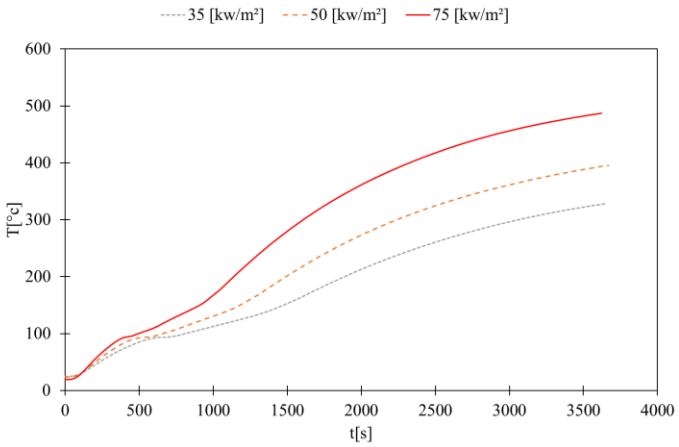

Figure 18: The temperature variation with time for the 7.75 [mm] thickness plate and dp 15 [mm].

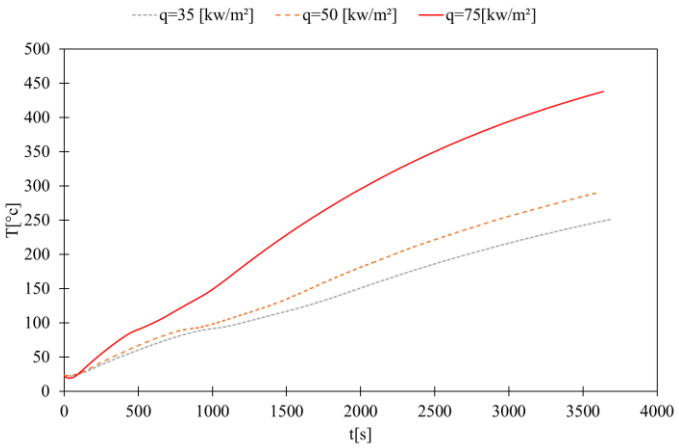

Figure 19: The temperature variation with time for the 14 [mm] thickness plate and dp 15[mm].

After getting result from above graphs, the following (Table 4) is obtained that shows the behavior of the steel plate under high temperature as the result for experimental test of protected steel with different thickness with the same insulation of 15 [mm] thickness and different heat flux in special temperature and special times.

The same thickness for protected carbon steel plate in q=35 [kw/m²] heat flux, when the time increases the temperature also increases; on the other hand, for 3.6 [mm] thickness steel plate, it has maximum temperature 400 [°c] with 3347 [s] time; more, it has maximum 300 [°c] temperature with 3057 [s] time for 7.75 [mm]. 14 [mm] thickness steel plate has maximum temperature 200 [°c] with 2717.5 [s] time. The same thing happens for both q=50 and q=75 [kw/m²]) heat flux.

So, finally on 400 [°c] for 4 [mm] thickness plate it takes 3347 [s] when the heat flux is q=35 [kw/m²]. On the mentioned temperature with heat flux it takes 2474 [s] when the heat flux is q=50 [kw/m²] and 1787 [s] when the heat flux is q=75 [kw/m²].

The steel is more protected when the thickness of steel is increased in the same heat flux and in another side we see that when the heat flux increases in the same thickness of steel plate, the steel takes short time for heating and in result it is less protected.

Table 4 - Results of experimental test of protected steel dp=15[mm].

q [kw/m²]	ds [mm]	Taverage [°c]				time[s]			
		900 [s]	1800 [s]	2700 [s]	3600 [s]	200 [°c]	300 [°c]	400 [°c]	500 [°c]
35	3.6	132.71	272.21	368.64	407.68	1407.5	1986	3347	/
	7.75	106.03	189.74	276.30	326.74	1886.5	3057	/	/
	14	88.02	136.12	198.94	247.27	2717.5	/	/	/
50	3.6	140.48	323.33	415.97	452.53	1219	1664.5	2474	/
	7.75	121.51	247.18	340.87	392.96	1490	2238.5	/	/
	14	92.86	163.79	235.83	290.13	2219.5	/	/	/
75	3.6	178.31	402.08	489.97	524.11	977.5	1299	1787	2896
	7.75	148.67	332.48	435.06	486.36	1138	1607	/	/
	14	135.78	270.47	369.16	435.98	1313	2035.5	3072	/

Here, for Figure 20, Figure 21 and Figure 22 and Table 5 it is 20 [mm] of thickness steel plate and we get different value of result like the same conclusion done in previous experimental test using protected carbon steel plate with 15 [mm] thickness of calcium silicate board.

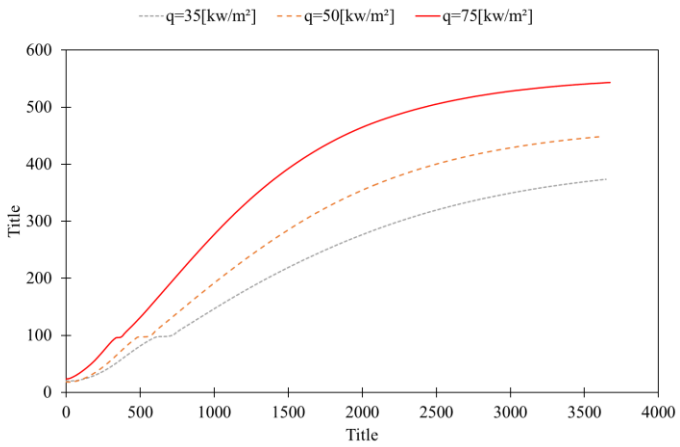

Figure 20: The temperature variation with time for the 3.6 [mm] plate and dp 20 [mm].

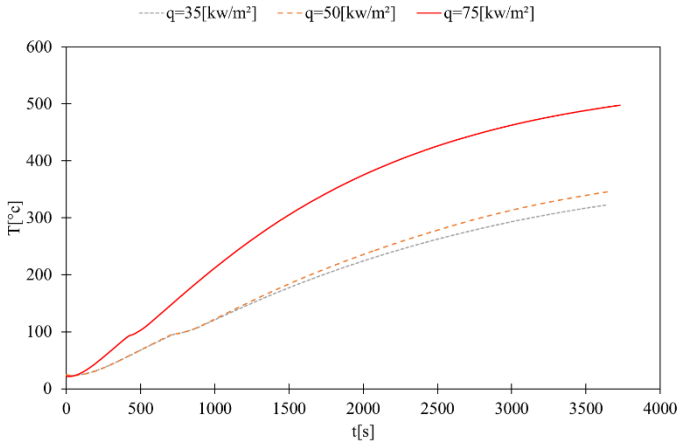

Figure 21: The temperature variation with time for the 7.75 [mm] thickness plate and dp 20 [mm].

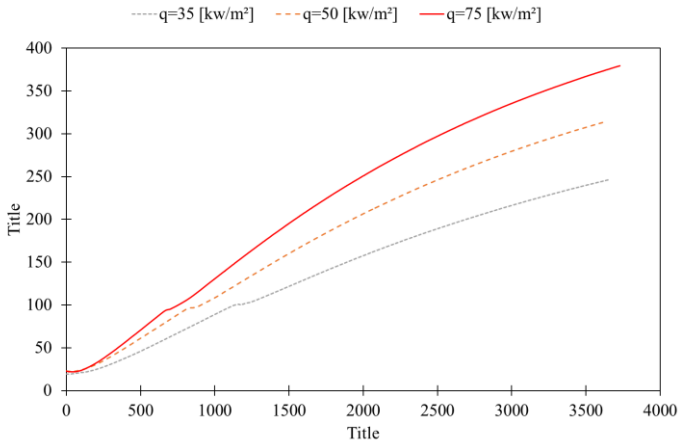

Figure 22: The temperature variation with time for the 14 [mm] thickness plate and dp 20 [mm].

Table 5 - Results of experimental test of protected steel dp=20[mm].

q [kw/m²]	ds [mm]	Taverage [°c]				time[s]			
		900 [s]	1800 [s]	2700 [s]	3600 [s]	200 [°c]	300 [°c]	400 [°c]	500 [°c]
35	3.6	130.67	255.26	332.98	372.38	1357.5	2251	/	/
	7.75	109.06	206.78	275.69	321.26	1728.5	3128	/	/
	14	80.17	143.72	200.43	244.04	2691.5	/	/	/
50	3.6	171.13	329.99	413.38	448.30	1040.5	1593	2496	/
	7.75	109.53	216.30	293.79	343.96	1643.5	2790.5	/	/
	14	99.31	188.81	260.15	312.62	1925	3356	/	/
75	3.6	249.03	440.47	516.12	542.24	733	1086.5	1543	2415
	7.75	190.73	349.89	442	492.92	943	1467.5	2222.5	/
	14	117.02	229.92	313.37	372.49	1539	2533	/	/

4.7 Comparison between the unprotected and protected carbon steel plate

Now, it is needed to make the last result of unprotected and protected carbon steel plate in the same graph, see graph of Figure 23 and Figure 24, that shows us the temperature variation with time, different heat flux and different thickness steel plate. The temperature is higher in unprotected carbon steel plate than protected carbon steel plate.

For instance, in Figure 23(a) for q=35, q=50 and q=75 [kw/m²] heat flux, the maximum temperature for unprotected steel plate is 610.55, 705.41 and 805.05 [°c]; for protected steel is 407.68, 452.53 and 524.11 [°c].

So, the result comes for 3.6 [mm] thickness protected steel plate is that the temperature decreases between 64.15% and 66.77% than unprotected steel plate, for 7.75 [mm] thickness protected steel plate it is between 55.00% and 66.46% and finally for 14 [mm] it is between 43.81% and 55.39% than unprotected steel plate.

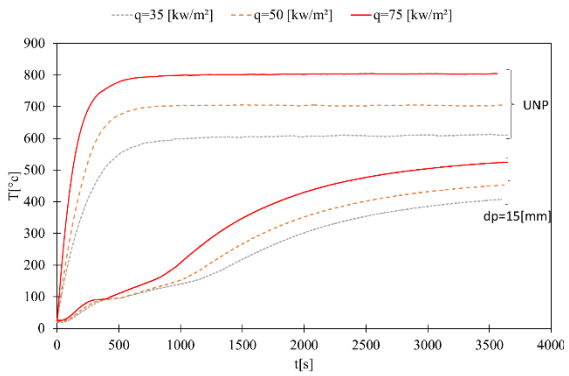

a) for 3.6 [mm] thikness plate

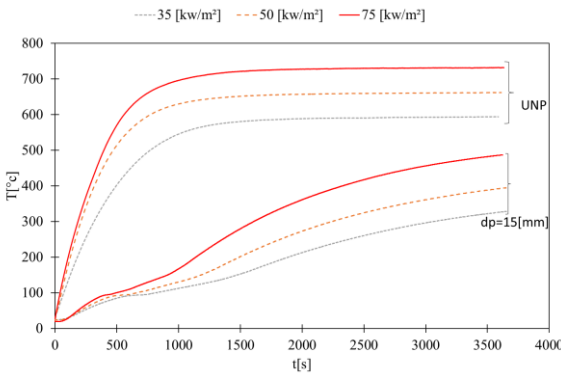

b) for 7.75 [mm] thikness plate

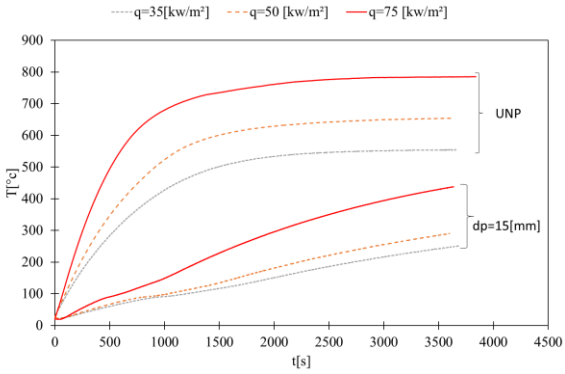

c) for 14 [mm] thikness plate

Figure 23: The temperature variation with time for unprotected and protected steel plate with insulation of 15 [mm] thickness.

Again, in Figure 24(a) for q=35, q=50 and q=75 [kw/m²] heat flux, it is the same thickness plate of Figure 23(a) what has the same maximum temperature for unprotected steel plate but now it is different insulation of 20 [mm] thickness. Moreover, about the maximum temperature for protected steel plate is 372.38, 448.30 and 542.24 [°c].

Here, for 3.6[mm] thickness protected steel plate the outcome we get is the temperature decreases between 60.99% and 67.35% than unprotected steel plate; for 7.75 [mm] it is between 51.91% and 67.35%; ultimately for 14 [mm] it is between 43.24% and 47.79% than unprotected steel plate.

In conclusion, from the above explanation and examples, the outcome comes for comparison between unprotected and protected steel plate that protected steel plate absorbs more temperature when the thickness of steel plate increases.

Figure 24 presents the comparison between protected and unprotected experimental test is the steel plate absorbs more energy when the thickness of steel plate increases.

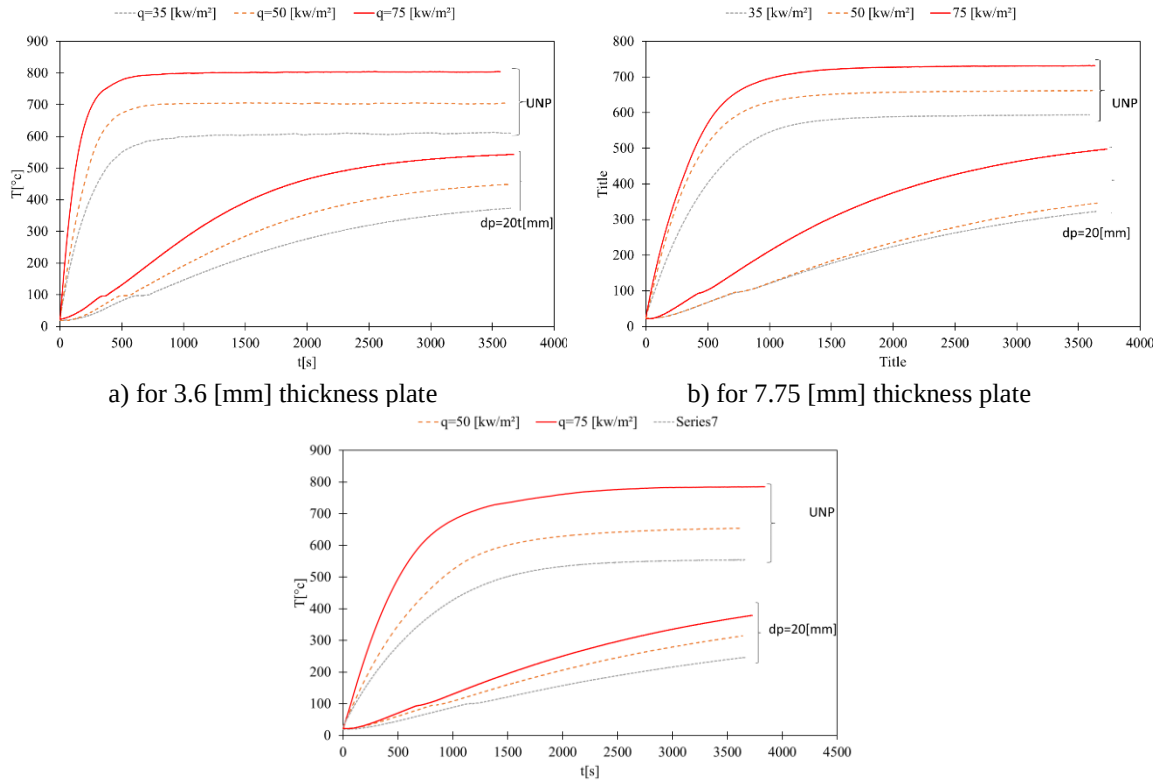

a) for 3.6 [mm] thickness plate

b) for 7.75 [mm] thickness plate

c) for 14 [mm] thickness plate

Figure 24: The temperature variation with time for unprotected and protected steel plate dp=20 [mm] thickness.

4.8 Measure the mass loss of calcium silicate board

An experimental test was made to know the mass loss of the insulation (calcium silicate board) and to measure the mass loss after 24h at 100 [°c], which is presented in Figure 25, we put the result in Table 6. Also, the thermal properties of the calcium silicate board were used in Table 9 and Table 10 and for the reaction of calcium silicate board in Table 8.

a) Mass before testing of thickness plate dp=20 [mm]

b) Mass after testing of thickness plate dp=20 [mm]

c) Mass before testing of thickness plate dp=15 [mm]

d) Mass after testing of thickness plate dp=15 [mm]

Figure 25 : Mass loss after 24 h at 100 [°c].

After measuring the mass loss of the calcium silicate board, results are presented in Table 6, where the mass loss of thickness dp = 15 [mm] is 15.9% moisture content, and 3% moisture content for the thickness dp = 20 [mm].

Table 6 – Mass loss of calcium silicate board with different thickness.

dp [mm]	M0 [g]	Mfinal [g]	Mass loss % moisture
15	117.1508	98.4774	15.9%
20	162.9786	158.1617	3%

Chapter 5: THE HEAT TRANFER EQUATION BY THE FINITE DIFFERENCE METHOD

5.1 Introduction

The finite difference method is one of several techniques for obtaining numerical solutions to Eq (10). In all numerical solutions, the continuous partial differential equation (PDE) is replaced with a discrete approximation. In this context, the word "discrete" means that the numerical solution is known only at a finite number of points in the physical domain. The number of those points can be selected by the user of the numerical method. In general, increasing the number of points not only increases the resolution (i.e., detail), but also the accuracy of the numerical solution, [14].

The discrete approximation results in a set of algebraic equations that are evaluated (or solved) for the values of the discrete unknowns.

The mesh is the set of locations where the discrete solution is computed. These points are called nodes, and if one is to draw lines between adjacent nodes in the domain the resulting image would resemble a net or mesh. Two key parameters of the mesh are Δx, the local distance between adjacent points in space and Δt, the local distance between adjacent time steps. For the simple examples considered in this article Δx and Δt are uniform throughout the mesh, [14].

In the next sections, the development of a numerical method will be presented and a solution is obtained for unprotected steel plates and plates with fire insulation.

5.2 Steel and insulation energy equation

Making a program in Matlab in which the compare between experimental and numerical result can be done.

The Eq(10) represents heat transfer equation in one dimension, for unprotected carbon steel plate q'''_{gen} = 0.

$$\rho_s c_s \frac{\partial T}{\partial t} = \frac{\partial}{\partial x}\left(k \frac{\partial T}{\partial x}\right) + q'''_{gen} \tag{10}$$

Also, Eq(10) works in initial boundary condition Eq(11) and boundary condition Eq(12) and Eq(13).

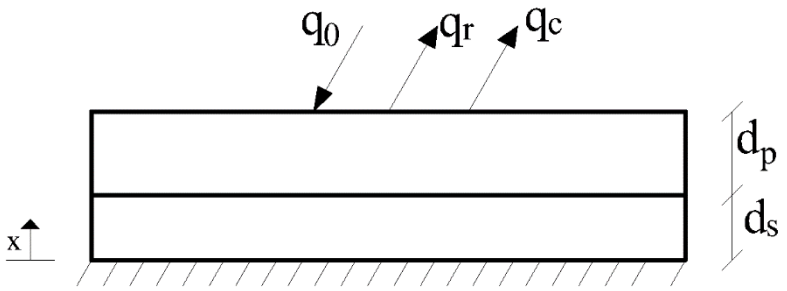

Figure 26 : Schematic drawing for specimen.

Initial boundary condition

If t=0 $$T(x, t = 0) = T_0 \tag{11}$$

boundary condition

If x=ds+dp $$k \frac{\partial T}{\partial x} = q_1(t) = \varepsilon q_0 - h(T - T_s) - \varepsilon\sigma(T^4 - T_s^4) \tag{12}$$

If x=0 $$k \frac{\partial T}{\partial x} = q_2(t) = 0 \tag{13}$$

In (14, x = ds is the thermal equilibiration (see Figure 26).

$T_{steel} = T_{ins}$ $$K_s \frac{\partial T_s}{\partial x} = K_{ins} \frac{\partial T_{ins}}{\partial x} \tag{14}$$

On the other hand, for protected carbon steel plate, Eq 14 is used to solve q'''_{gen} and to be calculated as a function of space and time according to the manufactured solution described, [15].

$$q'''_{gen} = H\frac{d\rho_s}{dt} \ , \tag{15}$$

Where Eq(15) shows the Generation equation, which is defined as a function of the pyrolysis rate q'''_{gen} and the heat-of-pyrolysis H. Here, H is positive value for endothermic pyrolysis.

By using Eq(15), the following equation can be obtained which is presented as Eq (16). When dt≈0, Eq (17) can be obtained from Eq (16)

$$dt \approx 0 \qquad \frac{d\rho_s}{dt} = \frac{d\rho_s}{dT} \times \frac{dT}{dt} \ , \tag{16}$$

By replacing Eq (17) in Eq (11) we obtain Eq (24) whereas, Eq (19) is obtained from Eq (18).

$$\rho c_p \frac{\partial T}{\partial t} - H\frac{d\rho_s}{dT} \times \frac{dT}{dt} = \frac{\partial}{\partial x}\left(k\frac{\partial T}{\partial x}\right) , \tag{17}$$

$$\frac{\partial T}{\partial t}\left(\rho c_p - H\frac{d\rho_s}{dT}\right) = \frac{\partial}{\partial x}\left(k\frac{\partial T}{\partial x}\right) , \tag{18}$$

If the phase transition takes place instantaneously at a fixed temperature, then a mathematical function is presented in Eq (19), [16].

$$\emptyset = \mathrm{U}(\mathrm{T} - T_f) \tag{19}$$

Where U is a step function with value zero when $T < T_f$ and otherwise $\delta(\mathrm{T} - T_f)$ is the direct delta function, whose value is infinity at the transition temperature T_f, but zero at all other temperatures, presented in Eq(20)

$$\frac{d\emptyset}{dT} = \delta(\mathrm{T} - T_f) \tag{20}$$

To alleviate this singularity the direct delta function can be approximated by the normal distribution function in which is presented in Eq (21)

$$\frac{d\emptyset}{dT} = \epsilon\pi^{-1/2} e^{-\epsilon^2(\mathrm{T}-T_f)^2}, \qquad \epsilon = \frac{1}{\sqrt{2}\Delta T} \tag{21}$$

where ΔT is one-half of the assumed phase change interval.

$$\rho_f = \rho_0 - \Delta\rho[0.5 + 0.5\tanh(\frac{T - T_f}{\Delta T_1})] \tag{22}$$

The similar specific heat is gained by affixing to the basis standard additional energy which is necessary because of volatilization of water or endothermic reaction or by deducting from base value energy released in time of endothermic reaction. Here, the base value normally depends on temperature but the extent is usually small. Hence, a certain value may be used if the appropriate variation is not available.

For this study, specific heat of the insulation (calcium silicate board) has four reactions. Each reaction has two equations or each reaction is determined by two equations (see Table 8).

When a fire protection material increases in temperature, external energy is required. The required external energy is reduced if the fire protection material generates heat through exothermic reaction or increased if the fire protection material undergoes endothermic reaction or if water is evaporated. The amount of energy required to raise the temperature of unit mass material by 1 [°C] is defined as the specific heat of the material. In simplistic heat transfer analysis, an equivalent specific heat may be used to represent the combined effects. The equivalent specific heat is obtained by adding to the base value additional energy that is required due to endothermic reaction or evaporation of water or by deducting from the base value energy that is released during exothermic reaction. The base value is usually temperature dependent. However, the range of this change is usually small. Therefore, if the precise variation is not available, a constant value may be used. To allow for heat generated/consumed during exothermic/endothermic chemical reactions and heat consumed

during water evaporation, a simple method is to distribute the energy involved through the temperature duration of the chemical reactions/water evaporation. The precise distribution may be difficult to quantify, but since the degree of accuracy required is not high, a triangular distribution may be conveniently used, [17], as represented in Figure 27.

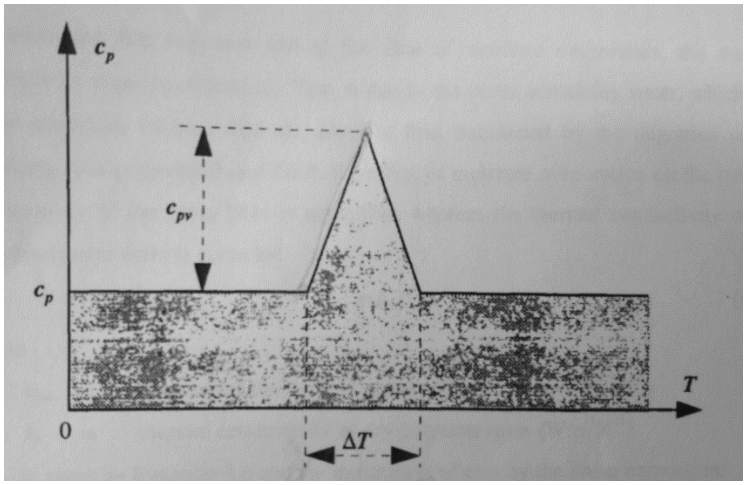

Figure 27: Triangular variation of specific heat during moisture evaporation.

The effect of moisture evaporation and other chemical reactions, on specific heat is simulated by assuming a simple mechanism driven only by the moisture concentration. It is assumed to take place during a temperature interval (ΔT) with a specific heat given by:

$$C_p = \mathrm{Cp}_0 + \mathrm{Cp}_v \tag{23}$$

The reaction starts at $T_{initial}$ is the primary temperature, T_{medium} is the temperature in peak water evaporation and T_{end} is the final temperature; T_2 is the temperature for insulation, Cp_0 is the initial specific heat, Cp_v is moisture specific heat.

$$Cp_v = 2H \times \frac{m_w}{\Delta T} \tag{24}$$

Where H is enthalpy for each reaction and moisture percentage is dependent on Table 8. More, ΔT is interval of each reaction, T_2 is temperature of insulation.

5.3 The finite difference method

Applying the finite-difference method to a differential equation involves replacing all derivatives with difference formulas. In the heat equation, there are derivatives with respect to time and derivatives with respect to space. Using different combinations of mesh points in the difference formulas results in different schemes. In the limit as the mesh spacing (Δx and Δt) go to zero, the numerical solution obtained with any useful1 scheme will approach the true solution to the original differential equation.

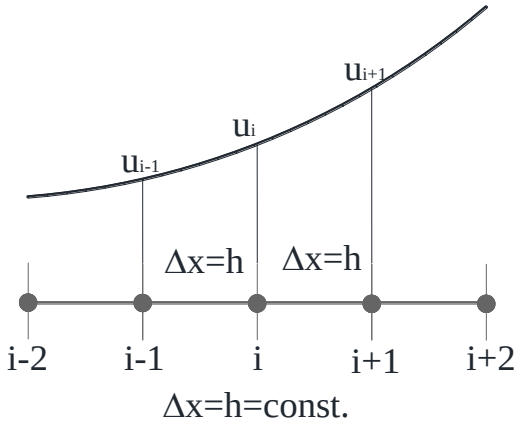

Figure 28: Finite Difference discretization of a function u or T.

Consider a Taylor series expansion u(x) about the point xi

$$u(x_i + \Delta x) = u(x_i) + \Delta x \frac{\partial u}{\partial x}\bigg|_{x_i} + \frac{\Delta x^2}{2}\frac{\partial^2 u}{\partial x^2}\bigg|_{x_i} + \frac{\Delta x^3}{3!}\frac{\partial^3 u}{\partial x^3}\bigg|_{x_i} + ... \qquad (25)$$

Solve for $(\partial u/\partial x)_{xi}$

$$u_x(x_i) = \frac{\partial u}{\partial x}\bigg|_{x_i} = \frac{u(x_i + \Delta x) - u(x_i)}{\Delta x} - \frac{\Delta x}{2}\frac{\partial^2 u}{\partial x^2}\bigg|_{x_i} - \frac{\Delta x}{3!}\frac{\partial^3 u}{\partial x^3}\bigg|_{x_i} + ... \qquad (26)$$

Substitute the approximate solution for the exact solution.

$$u_x = \frac{u_{i+1} - u_i}{\Delta x} + O(\Delta x) \tag{27}$$

This equation is called the forward difference formula for $(\partial u/\partial x)_{xi}$ because it involves nodes xi and xi+1. The forward difference approximation has a truncation error that is O(Δx). The size of the truncation error is (mostly) under our control because we can choose the mesh size Δx.

Finite difference approximations to higher order derivatives can be obtained with the additional manipulations of the Taylor Series expansion about u(xi).

$$u_{i+1} + u_{i-1} = 2u_i + \Delta x^2 \frac{\partial^2 u}{\partial x^2}\bigg|_{x_i} + \frac{2\Delta x^4}{4!}\frac{\partial^4 u}{\partial x^4}\bigg|_{x_i} + \ldots . \tag{28}$$

This is also called the central difference approximation, but it is the approximation to the second derivative.

$$u_{xx} = \frac{u_{i+1} - 2u_i + u_{i-1}}{\Delta x^2} + O(\Delta x^2) \tag{29}$$

5.4 Method of Lines

The author A. Vande Wouwer et al in 2001 discussed a system of PDEs with **u** which is a dependent vector. A vector is denoted by a bold face and a partial deriavative is denoted by a subscript. About the coordinates, Cartesian, Cylinderical and Spherical have components of (x, y, z), (r, θ, z) and (r, θ, φ), [18].

A general equation considering PDE problem is described where the equation encloses in one, two and three spatial dimensions plus time, Eq (30)

$$u_t = f(u), \qquad X_L < X < X_R, \; t > 0 \tag{30}$$

Here, $\mathbf{u_t} = \frac{\partial u}{\partial t}$ is the first order partial deriavative of **u** with respect to **t, u** is vector of dependent variables, t is initial value independent variable, **x** is boundary value independent variables, **f** is spatial differential operator **f** (**x**, t, **u**, $\mathbf{u_x}, \mathbf{u_{xx}}_{\ldots}$), [18].

For instance, the scalar advection Eq (31) comes from the spatial differential operator f if **f** (**x**, t, **u**, $\mathbf{u_x}, \mathbf{u_{xx}}_{\ldots}$) = $-vu_x$

$$\frac{\partial u}{\partial t} = -v\frac{\partial u}{\partial x} \tag{31}$$

Where $\mathbf{u_x} = \frac{\partial u}{\partial x}$ is the first order partial deriavative of **u** with respect to **x**, v is the velocity as constant.

PDE problems like Eq (30) is solved by the Method of Lines (MOL) which is a computational approach and that emanates into two different steps. Firstly, the spatial deriavatives and secondly, the resulting system of semi-discrete ODEs in the initial value variable is integrated in time, t.

According to the mentioned book, representing the MOL in Eq (31) gives us the Eq (33) using 2nd order centered FD in spatial deriavative at grid point i,

$$\frac{\partial u}{\partial x} = -v\frac{u_i - u_{i-1}}{2\Delta x} + O(\Delta x^2), i = 1, 2, \ldots\ , N \tag{32}$$

Then, substituting this estimation in Eq (31) with $v = 1$ gives a system of N ODEs Eq (33)

$$\frac{dui}{dt} = -\frac{u_{i+1} - u_{i-1}}{2\Delta x}, i = 1, 2, \ldots\ , N \tag{33}$$

Library ODE integrator can integrate the spatial grid index **i** what has the value similar to a system of N initial value of ODEs. Using the initial condition Eq (34) in boundary condition (i = **1** and **i = N)** gives us the fictitious point what is outside of the spatial domain, [18]. The integrator used in this work was the ode15s from the Matlab library.

About Spatial Discretization, to show the concept of upwinding in the book it is used as the approximation of $\frac{\partial u}{\partial x}$ in Eq (31) the first order, two-point upwind FD, Eq (35)

$$u(x,0) = f(x) \tag{34}$$

$$\frac{\partial u}{\partial x} = \frac{u_i - u_{i-1}}{\Delta x} + O(\Delta x), i = 1, 2, \dots \ , N \tag{35}$$

In Eq (36) the system of ODEs comes

$$\frac{dui}{dt} = -v\frac{ui - u\ i - 1}{\Delta x}, i = 1, 2, \dots \ , N \tag{36}$$

In Eq (35) the approximation for $\frac{\partial u}{\partial x}$ is called an upwind FD as it uses, besides to the point of the approximation, i, the point upwind, i -1 (for $v > 0$), but not the point downwind i+1.

More about time integration, a system of ODEs with widely separated eigenvalues called stiff ODEs is produced by spatial discretization. Δx – which is usually equal to the order of the highest spatial deriavative the time step restriction in a finely gridded region with small Δx that can be more acute than in coarsely gridded region as the durability limitation of an obvious time integration method is inversely proportional to some power of the grid spacing. A wide choice option of quality library ODE is available, even, one of the big benefits of the MOL approach to PDE systems is the scope to use the progression in ODE integrators and their associated codes, [18].

5.5 Comparison between experimental and numerical results of unprotected steel

When the program was prepared, for unprotected carbon steel plate the experimental results were used and obtained the following results transformed to graph charts and for the program see (ANNEX A3).

From Figure 29 to Figure 37, a variation of temperature is noticed through out the time and shows the numerical and experimental results with different thikness and different heat flux in which all results are similar. Whereas, a change in temperature is noticed in the curve of the numerical results what is presented in the Figure 31, Figure 34 and Figure 37 above 700[°C]. These changes are due to the presence of the peak of the specific heat of steel in 700[°C] that is presented in Figure 1.

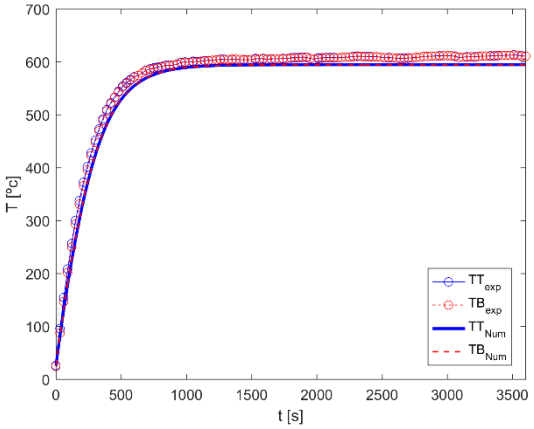

Figure 29: Results of the numerical method and experimental with thickness ds=3.6[mm] and heat flux q=35[KW/m²].

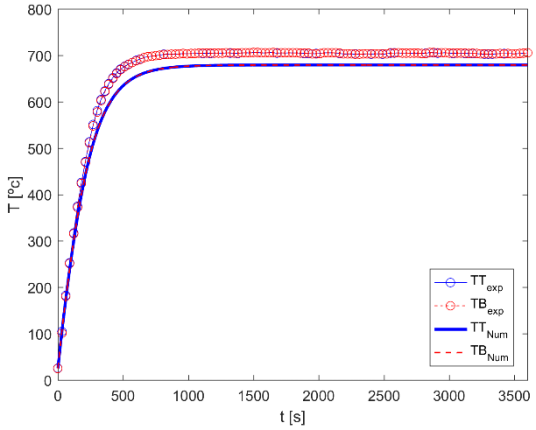

Figure 30: Results of the numerical method and experimental with thickness ds=3.6[mm] and heat flux q=50[KW/m²].

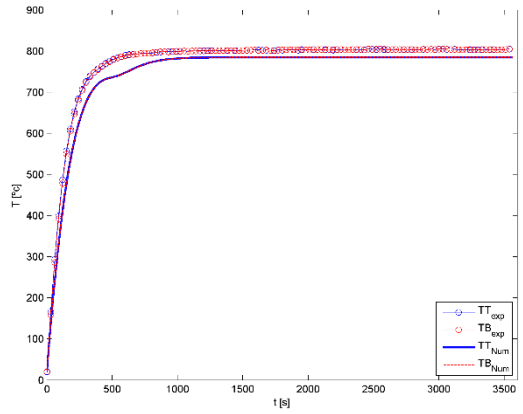

Figure 31: Results of the numerical method and experimental with thickness ds=3.6[mm] and heat flux q=75[KW/m²].

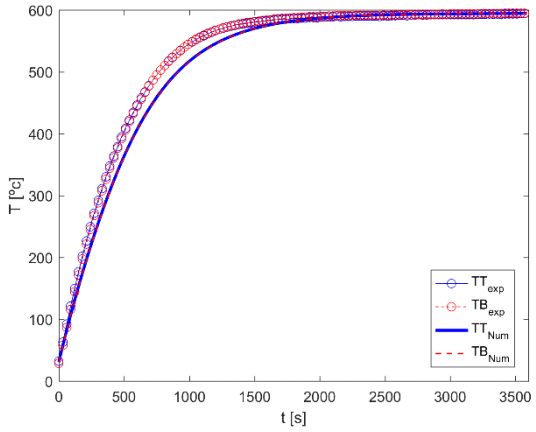

Figure 32: Results of the numerical method and experimental with thickness ds=7.75[mm] and heat flux q=35 [KW/m²].

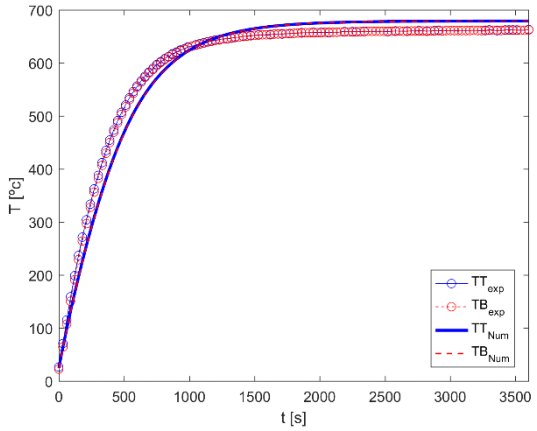

Figure 33: Results of the numerical method and experimental with thickness ds=7.75[mm] and heat flux q=50 [KW/m²].

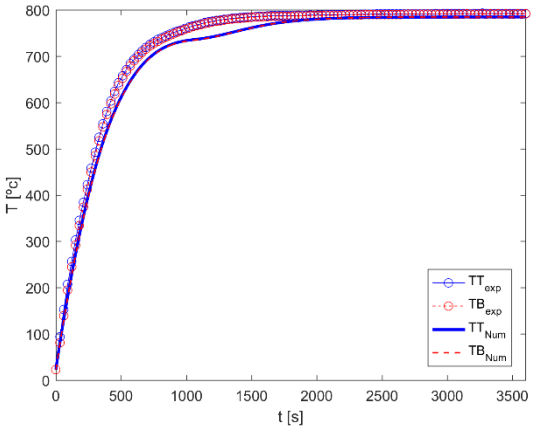

Figure 34: Results of the numerical method and experimental with thickness ds=7.75[mm] and heat flux q=75[kw/m²].

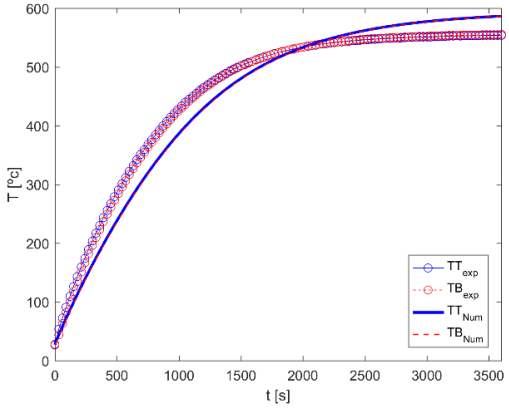

Figure 35: Results of the numerical method and experimental with thickness ds=14[mm] and heat flux q=35[kw/m²].

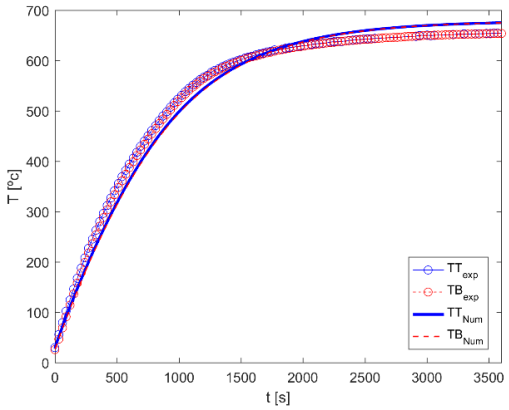

Figure 36: Results of the numerical method and experimental with thickness ds=14[mm] and heat flux q=50[kw/m²].

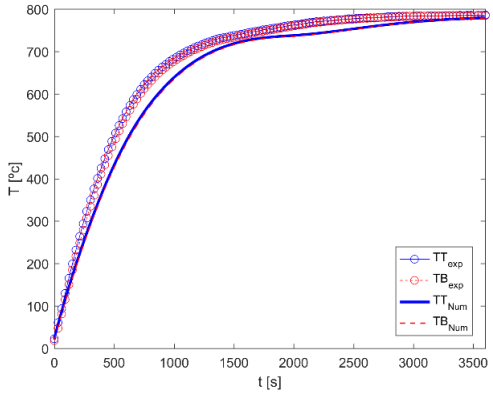

Figure 37: Results of the numerical method and experimental with thickness ds=14[mm] and heat flux q=75[kw/m²].

All results from the graphs were converted into values which were presented in Table 7. Analysis of results, showed variation of temperature through out time, thickness of steel plate and heat flux in which the temperature from carbon steel plate was very similar in the experimental and numerical result.

For the heat flux 35 q [kw/m²], the error for the experimental and numerical result is very similar dependent between 1.32% and 2.78% in 3.6 [mm] thickness steel plate. Moreover, in 7.75 [mm] thickness steel plate the error for both result is between 0.14% and 6.07%; in 14 [mm] it is dependent between 1.75% and 11.69%. The same thing happens for heat flux 50 and 75 q [kw/m²].

Table 7 – The result of temperature between experimental and numerical result for unprotected steel plate.

q[kw/m²]	ds[mm]		Temperature [°c]							
			900 [s]		1800 [s]		2700 [s]		3600 [s]	
			T_{-top}[°c]	T_{Bot}[°c]	T_{-top}[°c]	T_{Bot}[°c]	T_{-top}[°c]	T_{Bot}[°c]	T_{-top}[°c]	T_{Bot}[°c]
35	3.6	Ex	593	593	607	606	607	607	611	611
		Nu	585	585	594	594	594	594	594	594
	7.75	Ex	528	528	587	586	592	591	594	593
		Nu	497	496	582	582	593	593	593	593
	14	Ex	406	403	524	524	549	548	555	553
		Nu	359	356	514	513	569	568	569	568
50	3.6	Ex	702	702	705	705	704	704	704	704
		Nu	674	674	679	679	679	279	679	679
	7.75	Ex	620	619	656	656	660	660	662	661
		Nu	606	606	672	672	678	678	679	679
	14	Ex	542	537	639	638	654	653	657	656
		Nu	470	466	623	622	664	644	675	674
75	3.6	Ex	798	798	802	802	804	803	804	804
		Nu	779	778	784	784	784	784	784	784
	7.75	Ex	751	748	787	786	791	790	792	791
		Nu	726	725	775	775	784	784	784	784
	14	Ex	663	655	753	750	780	779	785	784
		Nu	610	605	733	731	760	759	779	778

5.1 Comparison between experimental and numerical result of protected steel

Table 8 represents the reaction of calcium silicate board where it absorbs 2330 [kj/kg] in a specific temperature [75°C] interval between 25 and 100 [°C] for evaporation of free water in first reaction and in second reaction it absorbs 1440 [kj/kg] in a specific temperature 125 [°C] interval between 100 and 400 [°C] for dehydration of calcium silicate board, Moreover, calcium silicate board absorbs 450 [kj/kg] in specific temperature 450 [°C] in interval between 400 and 600 [°C] for dehydration of calcium hydroxide , Finally the last reaction absorbs 750 [kj/kg] in a specific temperature 750°C between 600 and 1000 [°C] for decarbonation, [13].

Table 8 - Thermal Conductivity and Heat Capacity of Mild Steel vs. Temperature, [13].

ΔT[°c]	Treaction [°c]	Mass loss [kg]	Enthalpy [kj/kg]	Δmtotal[kg]
Evaporation of free water 25 to 100	75	9%	2330	12%
Dehydration of ‘calcium silicate hydrate get’ 100 to 400	125	23.5%	1440	
Dehydration of calcium hydroxide 400 to 600	450	21.5%	450	
decarbonation 600 to 1000	750	46%	750	

The both Table 9 and Table 10 show the thermal properties of calcium silicate board with different thickness.

Table 9 – Thermal properties of Promatect-200, [10].

T [°c]	λ [w/mk]	ρ [kg/m^3]
20	0.189	835

Table 10 - Thermal properties of Promatect-H, [19].

T[°C]	$\lambda_{w/mk}$	$C_p(400\ °C)_{KJ/KgK}$	ρ_{Kg/m^3}	moisture
20	0.17	0.92	870	5,95%
100	0.19			
200	0.21			

After making the program for the reaction of the calcium silicate board, it can be seen that the result in Figure 38 shows the parametric analysis of the moisture evaporation and for the Figure 38(a) we can see (1) is the first reaction (dT1= 5 [°c]), (2) is the second reaction (dT2= 150 [°c]), (3) is the third reaction (dT3= 100 [°c]) and (4) is the last reaction (dT4=200 [°c]). Finally, for Figure 38(b) and (c) the same interval for all reactions but changing the first reaction dT1 = 25 [°c] for (b) and 50 [°c] for (b).

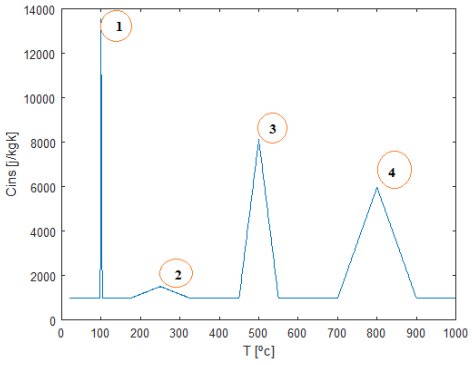

a) Interval for the first reaction dT1=5 [°c]

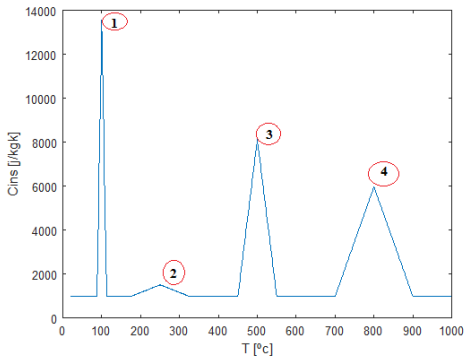

b) Interval for the first reaction dT1=25 [°c]

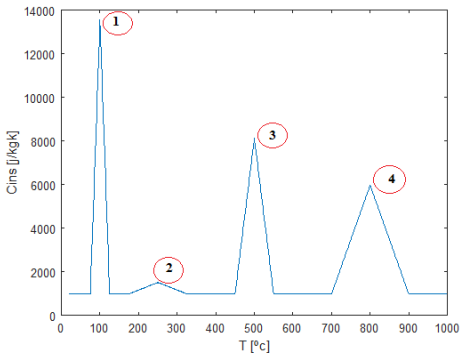

c) Interval for the first reaction dT1=50 [°c]

Figure 38: Parametric analysis of the moisture evaporation.

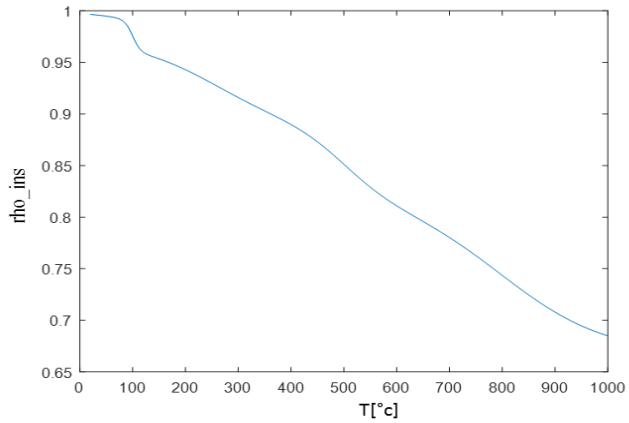

Figure 39 : Specific mass variation with temperature.

Now, after preparing the program, for protected carbon steel plate the experimental results are used and get the following results what are transformed to graph charts and for the program, it is the same of (ANNEX A3) but the difference for the function of 'Solve Parabolic', see (ANNEX A4).

According to curves presented in Figure 40, Figure 41 and Figure 42, evaporation of water occurred in range of temperature from 25 to 100[°C]. Above 100[°C], curves of the experiemental and numerical results increase normally through out time.

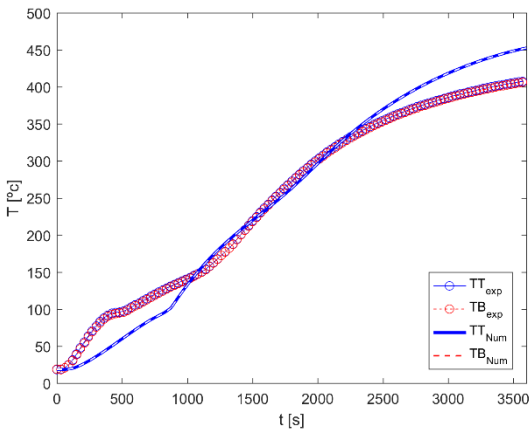

a)Temperature variation with time in heat flux q= 35 [kw/m²]

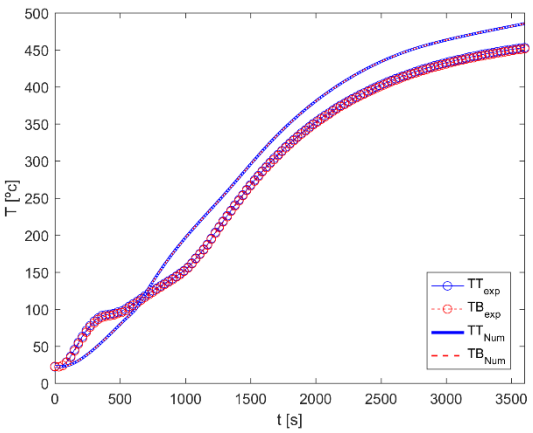

b)Temperature variation with time in heat flux q= 50 [kw/m²]

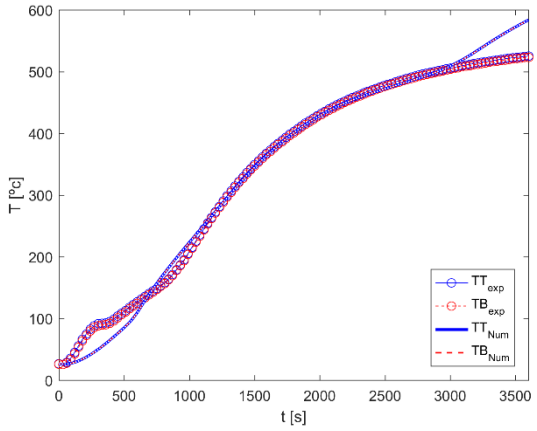

c)Temperature variation with time in heat flux q= 75 [kw/m²]

Figure 40: The experimental result and numerical result of protected carbon steel plate ds=3.6 [mm] with insulation dp=15 [mm] thickness.

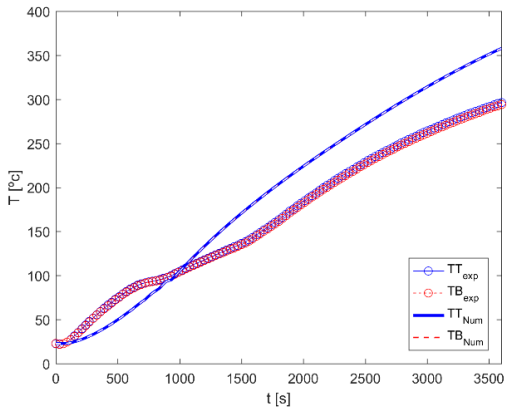

a)Temperature variation with time in heat flux q= 35 [kw/m²]

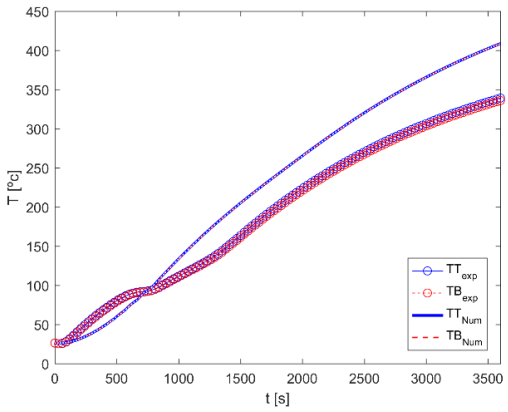

b)Temperature variation with time in heat flux q= 50 [kw/m²]

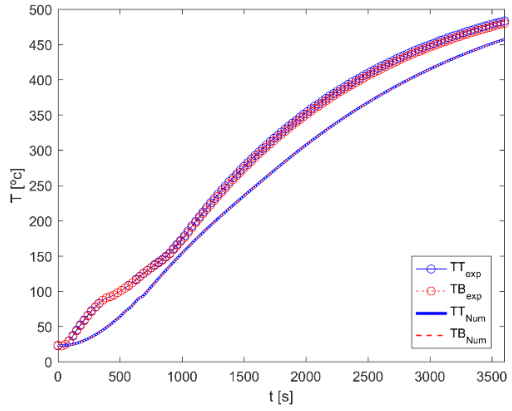

c)Temperature variation with time in heat flux q= 75 [kw/m²]

Figure 41: The experimental result and numerical result of protected carbon steel plate ds=7.75 [mm] with insulation dp=15 [mm] thickness.

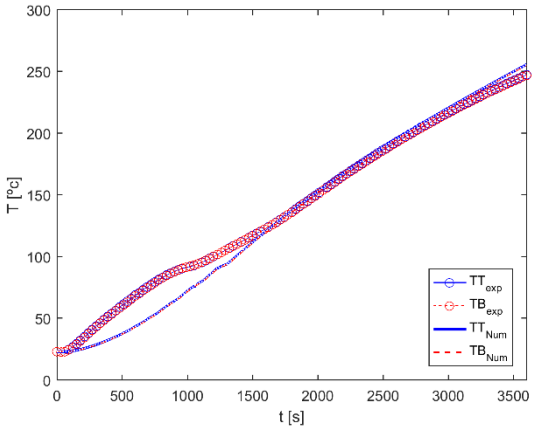

a)Temperature variation with time in heat flux q= 35 [kw/m²]

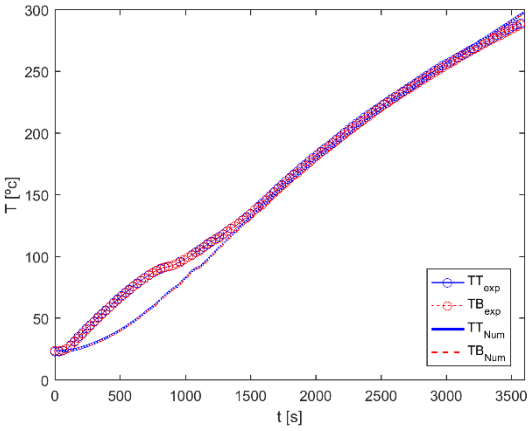

b) Temperature variation with time in heat flux q= 50 [kw/m²]

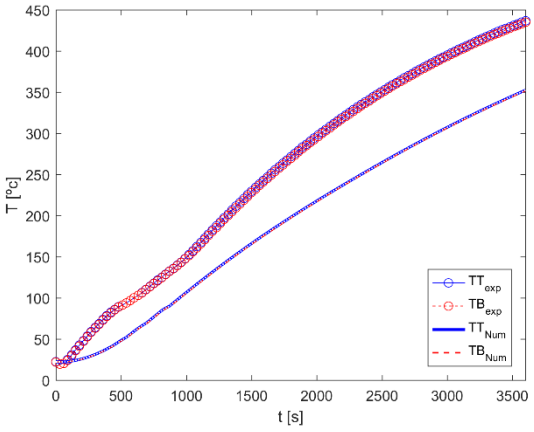

c) Temperature variation with time in heat flux q= 75 [kw/m²]

Figure 42: The experimental result and numerical result of protected carbon steel plate ds=14 [mm] with insulation dp=15 [mm] thickness.

As it was done in protected carbon steel plate, all curves were represented into values in the following table that shows the behavior of the steel plate under high temperature

For the heat flux 35 q [kw/m²], the error for the experimental and numerical result is similar dependent between 0.75% and 10.48% in 3.6 [mm] thickness steel plate. Moreover, in 7.75 [mm] thickness steel plate the error for both result is between 24.48% and 29.72%; in 14 [mm] it is dependent between 0.51% and 27.51%. Here, the same thing also happens for heat flux 50 and 75 q [kw/m²].

Table 11, also shows the results of experimental and numerical tests of protected steel plate with different thickness with the same insulation of 15 [mm] and different heat flux during 15, 30, 45 and 60 [min].

For the heat flux 35 q [kw/m²], the error for the experimental and numerical result is similar dependent between 0.75% and 10.48% in 3.6 [mm] thickness steel plate. Moreover, in 7.75 [mm] thickness steel plate the error for both result is between 24.48% and 29.72%; in 14 [mm] it is dependent between 0.51% and 27.51%. Here, the same thing also happens for heat flux 50 and 75 q [kw/m²].

Table 11 - The result of temperature between experimental and numerical result for protected steel plate with dp =15 [mm].

q[kw/m²]	ds[mm]		900[°c]		1800[°c]		2700[°c]		3600[°c]	
			T_{-top}[°c]	T_{Bot}[°c]	T_{-top}[°c]	T_{Bot}[°c]	T_{-top}[°c]	T_{Bot}[°c]	T_{-top}[°c]	T_{Bot}[°c]
35	3.6	Ex	133	132	272	271	369	367	407	405
		Nu	133	133	284	284	400	400	453	453
	7.75	Ex	98	97	163	161	243	241	294	292
		Nu	139	139	251	250	331	331	389	389
	14	Ex	88	87	136	135	199	198	245	245
		Nu	64	63	137	136	201	201	255	255
50	3.6	Ex	141	139	324	322	416	415	452	450
		Nu	174	174	351	350	442	448	485	485
	7.75	Ex	103	102	201	198	286	283	337	334
		Nu	117	117	241	241	339	339	408	408
	14	Ex	92	92	164	163	236	235	288	287
		Nu	73	72	160	160	233	233	289	297
75	3.6	Ex	178	177	403	401	491	488	524	522
		Nu	198	197	400	400	485	485	583	583
	7.75	Ex	154	152	325	322	427	412	481	478
		Nu	135	134	279	279	388	387	457	457
	14	Ex	135	135	271	269	370	368	434	432
		Nu	93	92	197	197	282	281	352	351

As it is done in previous part, all curves of the experimental and numerical results were presented in Figure 43 to Figure 51. The following graphs can be obtained for protected carbon steel plate with insulation of 20 [mm] thickness in which it presents the temperature

variation through out time of the experimental and numerical result where temperature of the experimental and numerical results is very similar.

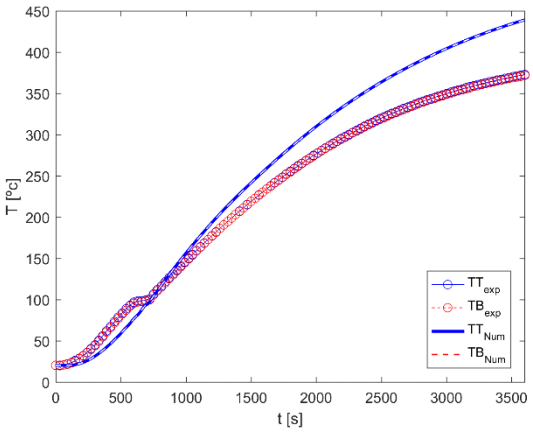

Figure 43: The experimental and numerical result of protected carbon steel plate with ds=3.6 [mm], dp=20 [mm] and q=35 [kw/m²].

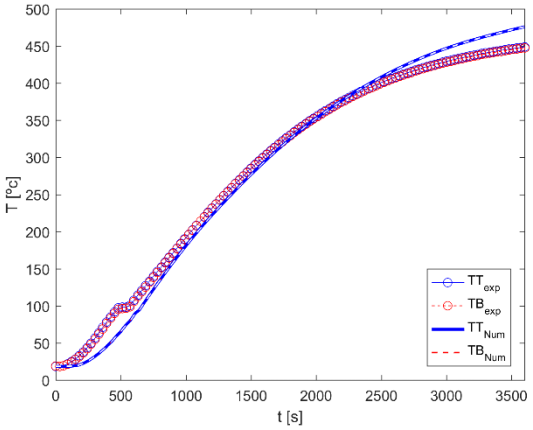

Figure 44: The experimental and numerical result of protected carbon steel plate with ds=3.6[mm], dp=20 [mm] and q=50 [kw/m²].

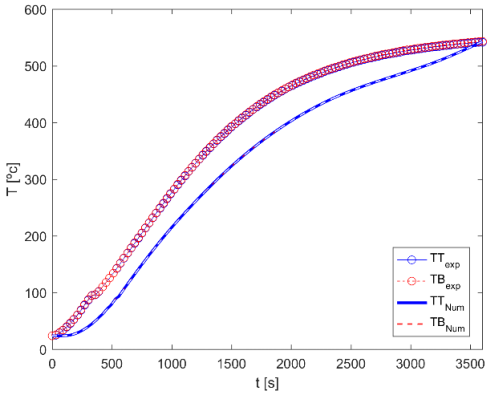

Figure 45: The experimental and numerical result of protected carbon steel plate with ds=3.6 [mm], dp=20 [mm] and q=75 [kw/m²].

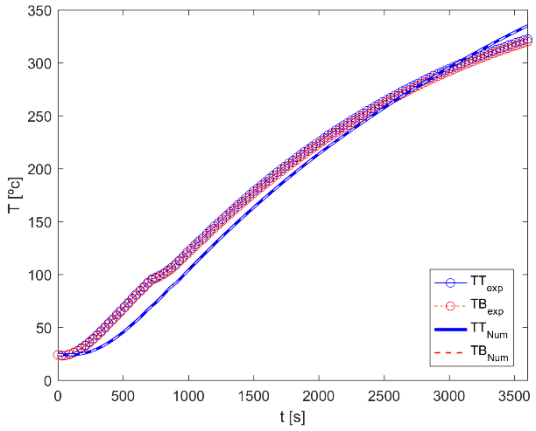

Figure 46: The experimental and numerical result of protected carbon steel plate with ds=7.75 [mm], dp=20 [mm] and q=35 [kw/m²].

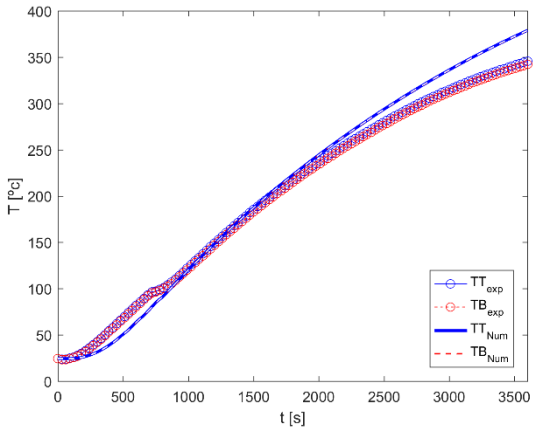

Figure 47: The experimental and numerical result of protected carbon steel plate with ds=7.75 [mm], dp=20 [mm] and q=50 [kw/m²].

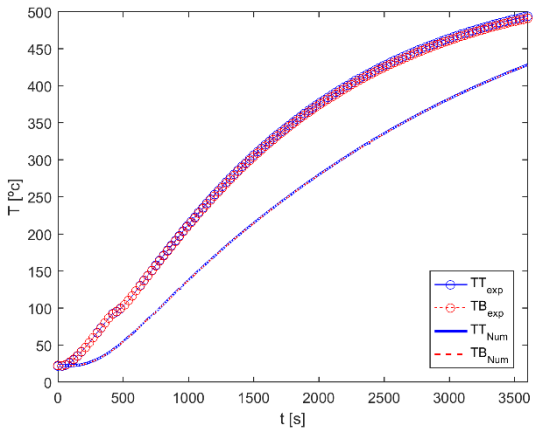

Figure 48: The experimental and numerical result of protected carbon steel plate with ds=7.75 [mm], dp=20 [mm] and q=75 [kw/m²].

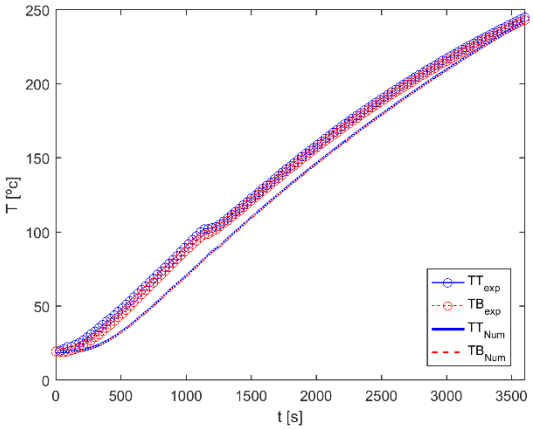

Figure 49: The experimental and numerical result of protected carbon steel plate with ds=14 [mm], dp=20 [mm] and q=35 [kw/m²].

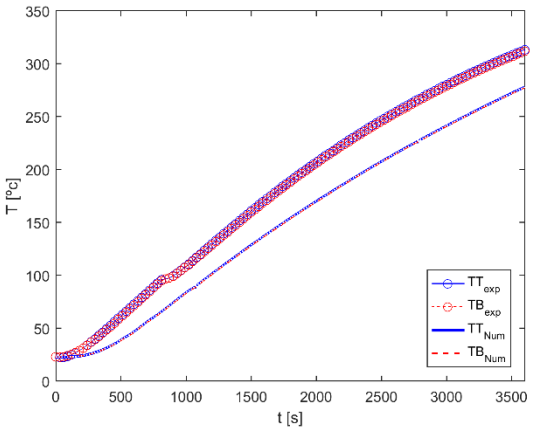

Figure 50: The experimental and numerical result of protected carbon steel plate with ds=14 [mm], dp=20 [mm] and q=50 [kw/m²].

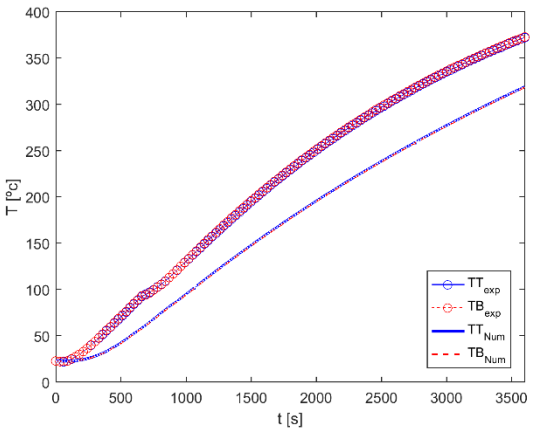

Figure 51: The experimental and numerical result of protected carbon steel plate with ds=14 [mm], dp=20 [mm] and q=75 [kw/m²].

Also, these graphs represent results into numerical values which are represented in the following Table 12 that shows the behavior of the steel plate under high temperature and shows the result of experimental and numerical tests of protected steel with different thickness in the same insulation of 15 [mm] and different heat flux during 15, 30, 45 and 60 [min].

The error for the experimental and numerical result is very similar dependent between 3.74% and 15.32% in 3.6 [mm] thickness steel plate for the heat flux 35 q [kw/m²]. More, in 7.75 [mm] thickness steel plate the error for both result is between 0.59% and 16.69%; in 14 [mm] it is dependent between 0.09% and 34.64%. For heat flux 50 and 75 q [kw/m²] the same thing happens too.

Table 12 - The result of temperature between experimental and numerical result for protected steel plate with dp =20 [mm].

q[kw/m²]	ds[mm]		900[s]		1800[s]		2700[s]		3600[s]	
			T_{top}[°C]	T_{Bot}[°C]	T_{top}[°C]	T_{Bot}[°C]	T_{top}[°C]	T_{Bot}[°C]	T_{top}[°C]	T_{Bot}[°C]
35	3.6	Ex	131	130	255	254	333	332	372	371
		Nu	136	136	284	284	381	381	439	439
	7.75	Ex	109	108	207	205	276	274	320	318
		Nu	91	91	194	194	273	272	335	334
	14	Ex	81	78	144	142	201	199	243	241
		Nu	62	62	132	131	131	191	242	241
50	3.6	Ex	171	170	330	329	414	412	448	447
		Nu	158	158	325	325	425	245	476	475
	7.75	Ex	110	108	217	214	295	292	344	340
		Nu	105	105	222	222	311	311	378	378
	14	Ex	99	99	189	188	260	259	311	309
		Nu	74	73	154	153	221	220	278	277
75	3.6	Ex	248	249	439	440	515	516	541	542
		Nu	189	189	374	374	471	471	542	542
	7.75	Ex	191	190	350	348	443	440	492	489
		Nu	121	120	255	354	355	355	428	428
	14	Ex	117	117	229	230	312	313	369	370
		Nu	84	83	177	176	254	253	319	318

Chapter 6: CONCLUSIONS AND FUTURE WORK

6.1 Main conclusions

The main target of our work was to make experimental test for protected and unprotected steel plate with different insulation, different thickness steel plate and different heat flux in cone calorimeter. For the protected carbon steel plate, two different insulations named Promatect-H and Promatect-200 (Calcium Silicate Board) with different thickness were used.

The experimental result for unprotected carbon steel plate, the temperature increases when the thickness of carbon steel plate increases.

For protected carbon steel plate, it is more protected when the thickness of plate increases in the same heat flux.

On the other hand, the comparison between protected and unprotected experimental test is the steel plate absorbs more energy when the thickness of steel plate increases.

Moreover, the comparison between experimental and numerical result is very similar for unprotected steel plate. For the heat flux 35 q [kw/m²], the error for the experimental and numerical result is very similar dependent between 1.32% and 2.78% in 3.6 [mm] thickness steel plate. Moreover, in 7.75 [mm] thickness steel plate the error for both result is between 0.14% and 6.07%; in 14 [mm] it is dependent between 1.75% and 11.69%. The same thing happens for heat flux 50 and 75 q [kw/m²].

Also, the comparison between the experimental and numerical result for protected steel plate is similar because the error dependent between 0.51% and 29.72% for 15[mm] and for 20[mm] thickness steel plate the error dependent between 0.09% and 35.64%.

The percentage for moisture evaporation is very important for protected carbon steel plate.

6.2 Future lines of investigation

In future, we can do more tests with different Calcium silicate board in the same thermal properties and different thickness. On other hand, we test Calcium silicate board for different thermal properties and the same thickness.

Use the Hot Disk and the Guarded Hot Plate methods in order to determine the thermal properties of different fire insulation materials.

Use different insulation (intumescent coating) for protected carbon steel plate.

REFERENCES

1. Thomas, G., *Thermal Properties of Gypsum Plasterboard at High Temperatures.* Fire Mater, 2002.
2. Bartholmai, M., R. Schriever, and B. Scharteln, *Influence of external heat flux and coating thickness on the thermal insulation properties of two different intumescent coatings using cone calorimeter and numerical analysis.* Fire Mater, 2003.
3. Adl-Zarrabin, B., L. Bostrom, and U. Wickstro, *Using the TPS method for determining the thermal properties of concrete and wood at elevated temperature.* Fire Mater, 2006.
4. Kodur, V.K.R. and A.M. Shakya, *Effect of temperature on thermal properties of spray applied fire resistive materials.* Fire Safety Journal, 2013.
5. Mróz, K., I. Hager, and K. Korniejenko, *Material solutions for passive fire protection of buildings and structures and their performances testing.* Procedia Engineering, 2016.
6. Li, G.-Q., et al., *Predicting intumescent coating protected steel temperature in fire using constant thermal conductivity.* Thin-Walled Structures, 2016.
7. Ferreiraa, D.M., et al., *Behaviour of non-loadbearing tabique wall subjected to fire – Experimental and numerical analysis.* Journal of Building Engineering, 2017.
8. Standardization, E.C.f., *Eurocode 3: Design of steel structures - Part 1-2: General rules - Structural fire design*. 2005: Brussels.
9. (CEN), E.C.f.S., *Eurocode 1: Actions on structures - Part 1-2: General actions - Actions on structures exposed to fire*. 2002: Brussels, Belgium.
10. Promat, *PROMATECT®-200-Fire resistant construction board*. 2016, Promat d.o.o.: Slovenia.
11. Promat, *PROMATECT®-H-Fire protective construction board*. 2016, Promat d.o.o.: Slovenia.
12. Normung, D.D.I.f., *ISO 13927 Plastics – Simple heat release test using a conical radiant heater and a thermopile detector*. 2003, European Committee for Standardization: Brussels.
13. Bentz, D.P. and K.R. Prasad, *Thermal Performance of Fire Resistive Materials I. Characterization with Respect to Thermal Performance Models.* Building and Fire Research Laboratory, 2007: p. 10.
14. Recktenwald, G.W., *Finite-Difference Approximations to the Heat Equation*, in *Mechanical Engineering*. 2004, Portland State University: Port-land, Oregon.

15. Ewing, M.E., T.S. Laker, and a.D.T. Walker, *Numerical Modeling of Ablation Heat Transfer*.

16. MUHIEDDINE, M., E. CANOT, and R. MARCH, *Various Approaches for Solving Problems in Heat Conduction with Phase Change*. Finite Volumes.

17. Wang, Y., et al., *Performance Based Fire Engineering of Structures*. 2017: CRC Press.

18. Wouwer, A.V., P.Saucez, and W.E. Schiesser, *Adaptive method of lines*. 2001.

19. Promat, *Calcium Silicate Insulation*. 2014, Promat GmbH: Germany. p. 35.

ANNEXES

A1. MATLAB PROGRAM FOR UNPROTECTED STEEL PLATES: Eurocode simplified method

```
%unprotected section
clc;
clear all; clc;
close all
rho_a=7850;
sigma=5,67*10^-8;
Ksh=1,0;
ds=0.0075;
Am= (0.100*0.100);
V=Am*ds;
SF=Am/V
alpha_c=25;
epsilon_m=0,7;
epsilon_f=1;
phi=1;
Tamb=20;
Ts (1) =Tamb;
dt=5;
time= [0:5:3600]
i=1
for t=time (2: end)
i=i+1;
Tg=20+345*log10(8*t/60+1)
h_net_c=alpha_c*(Tg-Ts(i-1))
h_net_r=phi*epsilon_m*epsilon_f*sigma*((Tg+273) ^4-(Ts(i-1) +273) ^4)
h_net=h_net_c+h_net_r
if 20<=Ts(i-1) & Ts(i-1) <600
    ca=425+7.73*10^-1*Ts(i-1)-1.69*10^-3*(Ts(i-1)) ^2+2.22*10^-6*(Ts(i-
1)) ^3
elseif 600<=Ts(i-1) & Ts(i-1) <735
    ca=666+13002/(738-Ts(i-1))
elseif 735<=Ts(i-1) & Ts(i-1) <900
    ca=545+17820/(Ts(i-1)-731)
else 900<=Ts(i-1) & Ts(i-1) <1200
    ca=650
end
dTs=Ksh*SF/(ca*rho_a) *h_net*dt
Ts(i)=Ts(i-1) +dTs
end
color='kgbcrm'; lines1= {'-';':';'-.';'-';':';'-.';};
marks='o*sxhph+^v<>';
Marker_Size=7;
```

```
plot(time,20+345*log10(8*time/60+1),'LineStyle', lines1{1},'Color',
color(5),'LineWidth',2)
hold on
plot (time, Ts,'LineStyle', lines1{1},'Color', color(3),'LineWidth',2)
xlabel ('t [s]'); ylabel ('T [°C]')
axis ([0 3600 0 1000]);
legend ('ISO834','ds=7.5 [mm]','location','SouthEast')
filename= strcat ('Unprotected ds=7_5 [mm]','.PNG');
print (figure (1), '-r300', '-dpng', filename);
%close all
```

A2. MATLAB PROGRAM FOR PROTECTED STEEL PLATE WITH GYPSUM BOARD: Eurocode simplified method

```
%protected section
clc;
clear all;
close all
dp=0.015
landa_p=0.2
rho_p=800
rho_a=7850
cp=1700
ds=0.010
fs=1/ds
Tamb=20;
Ts (1) =Tamb;
dt=5;
time= [0:5:3600]
i=1
Tg(i)=Tamb
for t=time (2: end)
i=i+1;
 Tg(i)=20+345*log10(8*t/60+1);
dTg=Tg(i)-Tg(i-1);
if 20<=Ts(i-1) & Ts(i-1) <600
    ca=425+7.73*10^-1*Ts(i-1)-1.69*10^-3*(Ts(i-1))^2+2.22*10^-6*(Ts(i-
1))^3;
elseif 600<=Ts(i-1) & Ts(i-1) <735
    ca=666+13002/(738-Ts(i-1));
elseif 735<=Ts(i-1) & Ts(i-1) <900
    ca=545+17820/(Ts(i-1)-731);
else 900<=Ts(i-1) & Ts(i-1) <1200
    ca=650;
end
phi=(cp*rho_p/(ca*rho_a)) *dp*fs;
dTs=(landa_p*fs*(Tg(i)-Ts(i-1)) *dt)/(dp*ca*rho_a*(1+phi/3)) -
(exp(phi/10)-1) *dTg;
if dTs<0
    dTs=0;
end
Ts(i)=Ts(i-1) +dTs;
end
color='kgbcrm'; lines1= {'-';':';'-.';'-';':';'-.';};
marks='o*sxhph+^v<>';
Marker_Size=7;
plot(time,20+345*log10(8*time/60+1),'LineStyle', lines1{1},'Color',
color(5),'LineWidth',2)
hold on
plot (time, Ts,'LineStyle', lines1{1},'Color', color(3),'LineWidth',2)
Xlabel ('t [s]') ; ylabel ('T [°C]')
axis ([0 3600 0 1000]);
legend ('ISO834','dp=15 [mm]','location','SouthEast')
filename= strcat ('protected section','.PNG');
print (figure (1), '-r300', '-dpng', filename);
```

A3. Main script of the matlab program for the finite difference method of steel plates with and without fire insulation

```
% Matlab Program: Heat Diffusion in one dimensional wire within the Fully
% Implicit Method
clear all
close all
clc
%... set global variables
global N2 N1 time time_id ncicles Tfire
global D1_1 D2_1 D1_2 D2_2 x1 x2 x dx0 L1 L2
global Ta sigma e_rad Q h
ds4=xlsread('ds4-35.xlsx','ds4-35EX','A4:c7294');
y=ds4 (:, 1); % TIME
z=ds4 (:, 2); % TOP TEMP
f=ds4 (:, 3) % bOTTOM TEMP
new_time= [0:30: max(y)]
NEW_Z=interp1(y, z, new_time)
NEW_F=interp1(y, f, new_time)
Tinit= (z (1) +f (1))/2 +273.15 % exp test initial temperature
% DISCRETIZATION
L1=0.0036/2 % Steel thckness
L2=0.0036/2 % protection thickness
xl=0;
xr=L1+L2
N1= 20;
N2=20;
x1=linspace (xl, L1, N1)';
x2=linspace (L1, xr, N2)';
x= [x1; x2]; % para não repetir o nó da fronteira
ni=length(x) % N1+N2-1
% Time intervals to study
dt=1;
tmax=max(y);
time= [0: dt: tmax]; %time in seconds. solution in 1h intervals
nj=length(time);
% Ambient temperature
Ta=20+273.15
sigma=5.6697e-8; % BoltzmanW/(m^2K^4)
e_rad=0.7 % 0.9 FOR THE GYPSUM INSULATION AND 0.7 FOR CARBON STEEL, 0.2
FROM vtt PAPER: Steel emissivity at high temperatures
h=20; % convective heat transfer coefficient w/m^2
Q=35e3; % external heat flux W/m^2
h=(1.4e-4*Q/1000+2.4e-6*(Q/1000) ^2) *1000; %from paper: Improved Method
for Analyzing Ignition Data from the Cone Calorimeter in the Vertical
Orientation
h=4; %natural convection
%######## cicle for the initial condictions
T0=Tinit; % Initial temperature
T1=T0*ones(N1,1);
T2=T0*ones(N2,1);
j=1;
T (:, j)=[T1;T2]';
% METHOD OF LINES WITH A FINITE DIFFERENCE SCHEME
% First and second derivatives for the layer 1: steel
D1_1=three_point_centered_D1(x1);
D2_1=three_point_centered_D2(x1);
% First and second derivatives of layer 2, insulation
D1_2=three_point_centered_D1(x2);
```

```
D2_2=three_point_centered_D2(x2);
for j=2: nj
options=odeset('RelTol',1e-6,'AbsTol',1e-6);
[tout, Tnew] = ode15s ('solve_parabolic', [time(j-1) time(j)], T (:, j-
1)); %...ODE solver
T (:, j)=Tnew(end,:)'; % temperature solution at time = time(itime)
T1 (:, j)=T(1:N1,j);% steel temperature
T2 (:, j)=T(N1+1:N1+N2,j); % %coating temperature
%hold on
plot (x, T (:, j)-273.15,'-b.','LineWidth',1)
axis ([0 max(x) 0 1.1*max (T2 (:, j) )]);
drawnow
%pause (1)
end
figure (2)
plot (new_time, NEW_Z,'-b','Marker','o')
hold on
plot (new_time, NEW_F,'--r', 'Marker','o')
hold on
plot (time (1: j), T2(N2, :)-273.15,'-b','LineWidth',2)
hold on
plot (time (1: j), T1(1, :)-273.15,'--r','LineWidth',1)
hold on
xlim ([0 3600])
%plot (texp, temp_exp,'b.','LineWidth',1)
%axis ([0 max(x) 0 1.1*max (T2(:, j) )]);
legend('TT_{exp}','TB_{exp}','TT_{Num}','TB_{Num}','location','SouthEast')
ylabel ('T [°c]'); xlabel ('t [s]');
filename= strcat ('Temp_ds= ', num2str((L1+L2) *1000), 'q= ',
num2str(Q/1000), '.PNG');
print (figure (2), '-r300', '-dpng', filename);
close all
out_time= [15 30 45 60] *60;
index1 = find (ismember (time, out_time));
TTop=T (N1+N2, index1)-273.15 %Numeric top temperatures
Tbot=T (1, index1)-273.15 %Numeric top temperatures
Save




function Tt = solve_parabolic (t, T);
%%% 1D heat equation with the Finite Difference Scheme
%     rho_ins.*cp_ins(T) dT/dt= d(kins(T) dT/dx) dx + heat_gener
%... set global variables
global N2 N1
global D1_1 D2_1 D1_2 D2_2 x1 x2 x dx0 L1 L2
global Ta sigma e_rad Q h
% Read the dependent variables value
T1=T (1: N1); % steel temperature
T2=T (N1+1: end); % %coating temperature
% steel material properties
for i=1: N1
[lambs(i,1), rho_s(i,1), cs(i,1)] = steel_prop(T1(i)-273.15);
end
alfa_s=lambs. /(rho_s.*cs); % steel difusivity
for i=1: N2
[lamb_ins(i,1), rho_ins(i,1), c_ins(i,1)] = steel_prop(T2(i)-273.15);
end
alfa_ins=lamb_ins./(rho_ins.*c_ins); % steel difusivity
% insulation thermal properties
```

```
%... First-order spatial derivative
T1x =D1_1*T1; %Zone 1
%... boundary conditions at x = 0 %K. Tx=0
T1x (1) =0;
%... First-order spatial derivative
T2x=D1_2*T2; %conductive heat flux
%... boundary conditions at x = xL
T2x(N2) = (1/lamb_ins(N2,1)). *(e_rad*Q -  h*(T2(N2)-Ta) sigma.
*e_rad.*(T2(N2). ^4-Ta. ^4));
%... Boundary condition at the steel interface
%convection at x=0
%T1x (1) =20*(T2(1)-Tamb)/lambs (1)
%... second-order spatial derivative
T1xx=D1_1*(lambs. *T1x);
%... temporal derivatives
T1t = (1. /(rho_s.*cs)). *T1xx; % steel layer
heat_gener=0. *ones(N2,1); % heat due to the moisture evaporation
T2t = (1. /(rho_ins.*c_ins)). *(D1_2*(lamb_ins.*T2x) +heat_gener); %
insulation
%... boundary conditions at x = xL1= x02 % Perfect thermal contact
between
%zone 1 and 2
T1t(N1) =lamb_ins (1,1) *T2x(1)-lambs(N1). *T1x(N1);
T2t (1) =T1(N1)-T2(1);
% Assemble the temporal derivatives
Tt (1:1: N1) =T1t;
Tt (N1+1:1: N1+N2) =T2t;
Tt=Tt';
```

```
function Tt = solve_parabolic (t, T); % with insulation
%%% 1D heat equation with the Finite Difference Scheme
%     rho_ins.*cp_ins(T) dT/dt= d(kins(T) dT/dx) dx + heat_gener

%... set global variables
global N2 N1
global D1_1 D2_1 D1_2 D2_2 x1 x2 x dx0 L1 L2
global Ta sigma e_rad Q h T_prev dt j_counter heat_gener cp0 rho0
moist_perc
% Read the dependent variables value
T1=T (1: N1); % steel temperature
T2=T (N1+1: end); % %coating temperature
% steel material properties
for i=1: N1
[lambs(i,1), rho_s(i,1), cs(i,1)] = steel_prop(T1(i)-273.15);
end
alfa_s=lambs. /(rho_s.*cs); % steel difusivity
 %insulation thermal properties

         lamb_ins = 0.189;
%... First-order spatial derivative
T1x =D1_1*T1; %Zone 1
%... boundary conditions at x = 0 %K. Tx=0
T1x (1) =0;
%... First-order spatial derivative
T2x=D1_2*T2; %conductive heat flux
%... boundary conditions at x = xL
T2x(N2) = (1/lamb_ins). *(e_rad*Q -  h*(T2(N2)-Ta) -sigma.
*e_rad.*(T2(N2). ^4-Ta. ^4));
```

```
%... Boundary condition at the steel interface
%... second-order spatial derivative
T1xx=D1_1*(lambs. *T1x);
%... temporal derivatives
T1t = (1. /(rho_s.*cs)). *T1xx; % steel layer

% source therm, heat generation
% specific heat calculation
 %insulation thermal properties
 delta_rho_t=moist_perc/0.09; delta_rho1=moist_perc;
delta_rho2=0.235*delta_rho_t; delta_rho3=0.215*delta_rho_t;
delta_rho4=0.46*delta_rho_t;
   Tf1=100+273.15; dT1=5;
 T1_ini=Tf1-dT1/2; T1_end=T1_ini+dT1; T1_m=Tf1;
  cp_m=2*2260000*moist_perc/dT1;
 for i=1: N2
     if T2(i)>=20+273.15 && T2(i)<=T1_ini
         c_ins(i,1) =cp0;
     elseif T2(i)>T1_ini && T2(i)<=T1_ini+dT1/2
         c_ins(i,1) =(cp_m-cp0)/(T1_m-T1_ini) *T2(i)+cp0-((cp_m-
cp0)/(T1_m-T1_ini)) *T1_ini;
     elseif T2(i)>=T1_ini+dT1/2 && T2(i)<T1_end
         c_ins(i,1) =(cp0-cp_m)/(T1_end-T1_m). *T2(i)+cp_m-((cp0-
cp_m)/(T1_end-T1_m)) *T1_m;
     else T2(i)>=T1_end
         c_ins(i,1) = cp0;
     end
 end
%second endothermic reaction
  Tf2=250+273.15; dT2=150;
 T2_ini=Tf2-dT2/2; T2_end=T2_ini+dT2; T2_m=Tf2;
  cp_m2=2*1440000*delta_rho2/dT2;
 for i=1: N2
     if T2(i)>=20+273.15 && T2(i)<=T2_ini
         c_ins(i,1) =c_ins(i,1);
     elseif T2(i)>T2_ini && T2(i)<=T2_ini+dT2/2
         c_ins(i,1) =(cp_m2-c_ins(i,1))/(T2_m-T2_ini) *T2(i)+c_ins(i,1) -
((cp_m2-c_ins(i,1))/(T2_m-T2_ini)) *T2_ini;
     elseif T2(i)>=T2_ini+dT2/2 && T2(i)<T2_end
         c_ins(i,1) =(c_ins(i,1)-cp_m2)/(T2_end-T2_m). *T2(i)+cp_m2-
((c_ins(i,1)-cp_m2)/(T2_end-T2_m)) *T2_m;
     else T2(i)>=T2_end
         c_ins(i,1) = c_ins(i,1);
     end
 end
 % third endothermic reaction
Tf3=500+273.15; dT3=100;
 T3_ini=Tf3-dT3/2; T3_end=T3_ini+dT3; T3_m=Tf3;
  cp_m3=2*5660000*delta_rho3/dT3;
 for i=1: N2
     if T2(i)>=20+273.15 && T2(i)<=T3_ini
         c_ins(i,1) =c_ins(i,1);
     elseif T2(i)>T3_ini && T2(i)<=T3_ini+dT3/2
         c_ins(i,1) =(cp_m3-c_ins(i,1))/(T3_m-T3_ini) *T2(i)+c_ins(i,1)-
((cp_m3-c_ins(i,1))/(T3_m-T3_ini))*T3_ini;
     elseif T2(i)>=T3_ini+dT3/2 && T2(i)<T3_end
         c_ins(i,1) =(c_ins(i,1)-cp_m3)/(T3_end-T3_m). *T2(i)+cp_m3-
((c_ins(i,1)-cp_m3)/(T3_end-T3_m)) *T3_m;
     else T2(i)>=T3_end
         c_ins(i,1) = c_ins(i,1);
     end
```

```
 end
 % fourth endothermic reaction
 Tf4=800+273.15; dT4=200;
 T4_ini=Tf4-dT4/2; T4_end=T4_ini+dT4; T4_m=Tf4;
  cp_m4=2*3890000*delta_rho4/dT4;
 for i=1: N2
     if T2(i)>=20+273.15 && T2(i)<=T4_ini
         c_ins(i,1) =c_ins(i,1);
     elseif T2(i)>T4_ini && T2(i)<=T4_ini+dT4/2
         c_ins(i,1) =(cp_m4-c_ins(i,1))/(T4_m-T4_ini) *T2(i)+c_ins(i,1) -
((cp_m4-c_ins(i,1))/(T4_m-T4_ini)) *T4_ini;
     elseif T2(i)>=T4_ini+dT4/2 && T2(i)<T4_end
         c_ins(i,1) =(c_ins(i,1)-cp_m4)/(T4_end-T4_m). *T2(i)+cp_m4-
((c_ins(i,1)-cp_m4)/(T4_end-T4_m)) *T4_m;
     else T2(i)>=T4_end
         c_ins(i,1) = c_ins(i,1);
     end
 end
rho_ins=rho0-rho0*moist_perc*(0.5+0.5*tanh((T2-Tf1)/(dT1/2)))-
rho0*delta_rho2*(0.5+0.5*tanh((T2-Tf2)/(dT2/2)))-
rho0*delta_rho3*(0.5+0.5*tanh((T2-Tf3)/(dT3/2)))-
rho0*delta_rho4*(0.5+0.5*tanh((T2-Tf4)/(dT4/2)));

T2t = (1. /(rho_ins.*c_ins)). *(D1_2*(lamb_ins.*T2x)); % insulation
%... boundary conditions at x = xL1= x02 % Perfect thermal contact
between
%zone 1 and 2
T1t(N1) =lamb_ins (1,1) *T2x(1)-lambs(N1). *T1x(N1);
T2t (1) =T1(N1)-T2(1);
% Assemble the temporal derivatives
Tt (1:1: N1) =T1t;
Tt (N1+1:1: N1+N2) =T2t;
Tt=Tt';
```